Multiples: signal or noise?

Arthur B. Weglein*

Right Running Head: Multiples: signal or noise?

March 25, 2016

*University of Houston, Department of Physics, Houston, Texas. E-mail: aweglein@central.uh.edu.

Abstract

Migration and migration-inversion are the seismic processing methods for structural determination and subsequent amplitude analysis, respectively. To-date, the most well founded and physically interpretable migration method is based on predicting a coincident source and receiver experiment at depth at time equals zero. In this paper, we extend that migration method, for heterogeneous media, and to accommodate two way propagation both in a local sense, at every point from the source to the target reflector and back from the reflector to the receiver, and globally, and separately, for each of the two legs from source to the reflector and from the reflector to the receiver. That provides the first migration method that avoids high frequency assumptions in both the imaging principle, and how it's implemented, and, hence, is equally effective at all frequencies at the target or reservoir.

This advance for two-way wave propagation migration then provides a tool to quantitatively, unambiguously and definitively define the role of primaries and multiples in migration.

The conclusion is that with data consisting of primaries and multiples, that for an accurate discontinuous velocity model that only primaries contribute to migration with the same image and inversion results independent of whether multiples or kept or removed.

On the other hand, for a smooth and continuous velocity model (that is generally assumed in practice) every multiple will result in a false, misleading and potentially injurious subsurface image and hence must be removed before migration. In practice we migrate with a smooth velocity model and hence multiples must be removed. When the collection of primaries is incomplete, a multiple can be used to provide an approximate image of an unrecorded primary. However, it

is always the migration of primaries that provides subsurface structure and amplitude information.

Introduction

In seismic exploration, signal is the part of the recorded seismic record (that is, the events) that is decipherable and useful for determining subsurface information relevant to the location and production of hydrocarbons. Migration and migration-inversion are the methods that are used to extract subsurface information from seismic reflection data. To carefully analyze and determine the role that primaries and multiples might play in determining structure and stratigraphic information, it is important for the purposes of this paper to review the different forms of migration and to examine their capabilities, characteristics and their strengths and limitations. That analysis and development of migration methods will then allow the careful examination of what precisely happens when primaries and multiples are input into methods designed to extract subsurface information. The outline of the paper is as follows: (1) migration concepts are reviewed; (2) the most well-founded, definitive and capable migration concept and imaging principle is extended for use in a volume with two way propagating waves; (3) that new migration method is then able for the first time to carefully examine the role of primaries and multiples in migration; and (4) we provide an analytic analysis that demonstrates that for an accurate discontinuous velocity model, that multiples don't contribute to imaging. For a continuous velocity model, multiples produce false images, and, hence, in practice

need to be removed before imaging and inversion; (5) only primaries are needed for migration and migration-inversion, but when the data collection is incomplete a multiple can be used to find an approximate image of an unrecorded subevent primary of the multiple.

A more detailed history of the evolution of migration concepts, with a large number of additional and relevant references, can be found in, e.g., Stolt and Weglein (2012).

Migration: the evolution of concepts and algorithms

To begin, "signal" within the context of exploration seismology, and for the purpose of this paper, refers to the events in seismic recorded data used for extracting subsurface information. Since migration and migration-inversion are the methods used to determine subsurface structural and stratigraphic information from recorded seismic data it is essential for the purpose of this paper to examine these procedures. Methods that employ the wave equation for migration have two ingredients: (1) a wave propagation concept and (2) an imaging condition. A useful reference for our purpose is Claerbout (1971) where he described three imaging conditions for seismic migration. He combined these imaging conditions with one-way wave propagation concepts to determine structure at depth. The three imaging conditions are: (1) the exploding reflector model, (2) the space and time coincidence of upgoing and downgoing waves, and (3) the predicted coincident source and receiver experiment at depth, at time equals zero. Although others pioneered and contributed to these imaging conditions (for example, D. Lowenthal, J.

Sherwood, F. Muir, and R. H. Stolt), we will refer to these original imaging conditions as Claerbout I, II and III. Claerbout I only relates to stacked or zero offset data whereas Claerbout II and Claerbout III are valid for prestack data. The objective of these three imaging conditions was basically limited to determining structure, with the exception that the third condition provided an angle averaged plane wave reflection coefficient. These three imaging principles will give equivalent results for a normal incident plane wave on a horizontal reflector. For anything more complicated (and more realistic), starting with a single shot record and a single horizontal reflector, they will not be equivalent in terms of structural and amplitude accommodation, image interpretability, consistency and fidelity. The third imaging condition stood alone in terms of clarity and definitiveness and in its potential, allowing Stolt and his colleagues to extend the original for the more physically complete and accommodating structural models, and in addition provides a detailed angle dependent amplitude analysis at the target, for both specular and non-specular reflection. The third imaging condition predicts an actual seismic experiment at depth, and that predicted experiment consists of all the events that experiment would record, if you had a source and receiver at that subsurface location. That experiment would have its own recorded events, the primaries and multiples for that predicted experiment. Stolt and his colleagues (Clayton and Stolt, 1981; Stolt and Weglein, 1985; Stolt and Benson, 1986; Weglein and Stolt, 1999; Stolt and Weglein, 2012) then provided the very significant generalization and extension [for one way waves] of the Claerbout source and receiver experiment imaging condition (Imaging condition III) to allow for a non-coincident source and receiver at time

equals zero, to realize both structural and inversion objectives. Linear inverse scattering theory played an essential role in that evolution, facilitating the extension, generalization and merging of these distinct and separate earlier migration and AVO concepts into fully multidimensional structural and amplitude analysis capability. Due to causality, the offset dependence, at time equals zero, is highly localized about zero offset. The character of that singular function, sharply peaked in offset, is smooth in the Fourier conjugate space of offset wave-number, where the extraction of angle dependent plane wave reflection information naturally occurs. The latter extension and generalization produced migration-inversion (Stolt and Weglein, 1985), or first determining where anything changed (migration) followed by what specifically changed (inversion) at the image location.

Recently, several papers by Weglein and his colleagues (Weglein et al., 2011b,c; Liu and Weglein, 2014) provided the next step in the evolution of migration based on the Claerbout predicted source and receiver experiment imaging condition (Imaging condition III), extending the prediction of the source and receiver experiment to a volume within which there are two way propagating waves. The latter method of imaging based on Imaging condition III for a medium with two way propagating waves, plays a central role in the analysis of this paper. Carefully analyzing the role of primaries and multiples in imaging calls for a starting point with a firm math-physics framework and foundation, without ad hoc ingredients and steps, and requires the most definitive and quantitative of migration concepts applied in a volume with two way propagating waves. The new two way wave propagating migration extension of Stolt's generalization of Claerbout III is the

clear and only choice. The predicted experiment, in the volume is realized by calling upon Green's theorem and a Green's function that together with its normal derivative vanishes on the lower portion of the closed surface.

All current RTM methods, for two way propagating waves, are extensions and/or variants of the second of Claerbout's imaging conditions, and do not correspond to Claerbout's imaging condition III.

Variants and extensions of the original Claerbout II imaging principle (see, e.g., Stolt and Weglein, 2012, pp. 78-79 and Zhang et al., 2007) can provide a geometric optics approximate reflection coefficient but only Claerbout III imaging can produce an actual plane wave reflection coefficient as a function of angle for a specular reflector and can generalize to a point reflectivity for imaging and inverting specular or non-specular reflections. Claerbout III imaging has no problem imaging above or beneath (and finding the reflection coefficient from below) a rapid change in velocity in contrast to Claerbout II. The well-known artifacts in Claerbout II imaging when migrating with a discontinuous velocity model (e.g., so called Rabbit ears) simply do not occur in Claerbout III imaging. Claerbout II imaging, for a single source and a single receiver, produces a travel time curve of candidate images. That's a clear indication of a high frequency ray theoretic assumption that's intrinsic to Claerbout II and all its variants and extensions. Claerbout III imaging never produces candidate images (at any step or stage) and doesn't have a high frequency asymptotic ray theoretic assumption. For Claerbout III, the predicted coincident experiment at a point in the subsurface determines directly whether or not the point corresponds to structure or not: there are no candidate points where structure might (or might not) exist. If we want to

isolate and to determine the role different events play in a migration method, and thereby to define which events are signal, and which events are noise, then a migration method that depends on the coherent constructive interference of candidate images begins with a certain intrinsic vagueness and ambiguity on what constitutes an image, before we consider what events contribute to an image. That is in comparison with the Claerbout III imaging and the predicted coincident source and receiver experiment at depth at $t = 0$, with its definitive yes or no for every potential subsurface point as structure, and avoids the blurriness and ambiguity with Claerbout II. The lack of ambiguity and blurriness in the Claerbout III imaging principle, drives/supports the examination of the role of primaries and multiples using Claerbout III.

Migration of two-way propagating waves

One doesn't have to look very far to find an example with the need for a predicted experiment at depth at points in a volume where there is two way wave propagation. Imaging from above and below a single horizontal reflector already requires two way wave propagation for Claerbout's predicted experiment imaging condition. Predicting a source and receiver experiment to locate and to determine the reflection coefficient from above, and, separately, from below, a single reflector requires predicting a source and receiver experiment inside a volume with two way propagating waves, that is, two way wave migration, since the reflection data is upgoing (to a source and receiver experiment located) above the reflector and is downgoing (to that

experiment when the source and receiver are located) below the reflector. Of course, the addition of, for example, multiples and/or diving waves also represent examples of two way wave propagation in the region where you want to predict the seismic experiment at depth. Wave propagation is one way only in a homogeneous medium. Assuming one way wave propagation at a point in any inhomogeneous medium (even if slowly varying) is a high frequency assumption. High frequency assumptions can enter migration methods in various obvious and subtle ways. Asymptotic approximations, and stationary phase approximations of integrals and ray theoretic ingredients are obvious high frequency approximations. That the Claerbout II imaging condition itself is intrinsically high frequency is less than obvious. However, the candidate travel time images that reside within the Claerbout II method are the unambiguous and definitive indicator of that assumption and character. All current RTM methods are based on the original or extensions of Claerbout II imaging and share the intrinsic approximate asymptotic high frequency nature of its imaging condition, independent of how it is implemented. In contrast, the Claerbout III imaging principle is not intrinsically asymptotic or making a high frequency approximation. In addition, in this paper, we describe how to avoid asymptotic approximations in how the Claerbout III imaging is implemented. That combination of imaging principle and method of implementation then provides the first migration method and strategy that is equally effective at all frequencies at the target/reservoir.

As we mentioned, migration methods that employ the wave equation have two ingredients: (1) a wave propagation or prediction model and (2)

an imaging condition. As we also mentioned above, for the purposes of this discussion, we are going to adopt the Claerbout III imaging condition for its clarity, quantitative and interpretable information value. In the next section, we describe the evolution of the prediction of the source and receiver experiment component of Claerbout imaging condition III. It is only the wave propagation model and component that has recently been progressed (to allow for two way propagating waves in the volume), not the Stolt extended Claerbout III imaging condition itself.

To predict the source and receiver experiment at depth

The classic well established mathematical physics foundation for predicting a wavefield inside a volume from (measured) values of the field on the surface surrounding the volume was provided by Green (1828) and is known as Green's theorem. In the next several sections, we describe the evolution and application of Green's theorem for predicting the source and receiver experiment at depth. In that evolution, we will begin with: (1) the original infinite hemisphere volume model, then (2) the reasoning, need for, and description of the finite volume model for one way waves, and finally, (3) the need for and description of the finite volume model prediction of the source and receiver experiment for two way waves. The third step in this evolution is a fairly recent development (Weglein et al., 2011b, Weglein et al., 2011c, and F. Liu and Weglein, 2014).

The material presented below on the evolution of the predicted source

and receiver experiment has been published previously in the cited references in the last paragraph. We cite and follow those references, but include that in this paper, for: (1) pedagogic value and logical presentation, and (2) to make this paper self-contained, and (3) because it plays such a critical role in Claerbout imaging III, which in turn is essential for understanding one of the key new messages (for migrating primaries and multiples) that this paper is communicating.

Extending Stolt's generalized Claerbout III imaging to accommodate two way propagating waves

In this section, we present a new Green's theorem method for predicting a source and receiver experiment at depth inside a finite volume (where waves are two way propagating both between the source and the reflector and from the reflector back to receivers on the measurement surface), from recorded source and receiver data. To follow and understand this new development we encourage the reader to see the review of Green's theorem wave field predictions in Appendices I-IV.

This migration method will then be used to provide a definitive response to the coupled/linked questions: "the role of primaries and multiples in migration and migration-inversion" and "multiples: signal or noise?"

Predicting the source-receiver experiment at depth where the velocity configuration is $c(x, y, z)$

For a receiver predicted at a point (x, y, z) for determining $P(x, y, z, x_s, y_s, z_s, \omega)$, call on the Green's function, G_0, that satisfies

$$\left\{\nabla'^2 + \frac{\omega^2}{c^2(x', y', z')}\right\} G_0(x', y', z', x, y, z, \omega)$$
$$= \delta(x - x')\delta(y - y')\delta(z - z') \quad (1)$$

for a source at (x, y, z). P is the physical/causal solution satisfying

$$\left\{\nabla'^2 + \frac{\omega^2}{c^2(x', y', z')}\right\} P(x', y', z', x_s, y_s, z_s, \omega)$$
$$= A(\omega)\delta(x' - x_s)\delta(y' - y_s)\delta(z' - z_s). \quad (2)$$

As a first step, we want to predict P for a point (x, y, z) in the volume V, for the actual/original source at (x_s, y_s, z_s). For (x, y, z) in V, arrange for G_0 and $\nabla' G_0 \cdot \hat{n}'$ to be zero for (x', y', z') on the lower surface S_L and the walls S_W of the finite volume. The solution for G_0 in V and on S can be found by a numerical modeling algorithm where the "source" is at (x, y, z) and the field, G_0, and $\nabla G_0 \cdot \hat{n}$ at (x', y', z') are both imposed to be zero on S_L and S_W. Once that data is computed (modeled) for a source at (x, y, z) for $G_0(x', y', z', x, y, z, \omega)$ [for every output predicted receiver point, (x, y, z), from Green's theorem for P] where G_0 satisfies Dirichlet and Neumann conditions for (x', y', z') on S_L and S_W we output $G_0(x', y', z', x, y, z, \omega)$ for (x', y', z') on S_U (the measurement surface).

With that G_0, use Green's theorem to predict the receiver experiment at depth (with the original/actual source at (x_s, y_s, z_s))

$$\begin{aligned} & P(x, y, z, x_s, y_s, z_s, \omega) \\ = & \int_{S_g} \left\{ \frac{\partial G_0^{DN}}{\partial z'}(x, y, z, x', y', z', \omega) P(x', y', z', x_s, y_s, z_s, \omega) \right. \\ & \left. - \frac{\partial P}{\partial z'}(x', y', z', x_s, y_s, z_s, \omega) G_0^{DN}(x, y, z, x', y', z', \omega) \right\} dx' dy', \end{aligned} \tag{3}$$

where z' = fixed depth of the cable and (x_s, y_s, z_s) = fixed location of the source. S_g is the upper (measurement) surface containing receivers for a fixed shot on the measurement surface. This predicts the receiver at (x, y, z), a point below the measurement surface in the volume V (for a source on the upper (measurement) surface) in terms of measurements on the upper surface, S_u.

Now predict the experiment corresponding to both the receiver and the source at depth, by invoking reciprocity and performing a Green's theorem surface integral over sources

$$\begin{aligned} & P(x_g, y_g, z, x, y, z, \omega) \\ = & \int_{S_s} \left\{ \frac{\partial G_0^{DN}}{\partial z_s}(x, y, z, x_s, y_s, z_s, \omega) P(x_g, y_g, z, x_s, y_s, z_s, \omega) \right. \\ & \left. - \frac{\partial P}{\partial z_s}(x_g, y_g, z, x_s, y_s, z_s, \omega) G_0^{DN}(x, y, z, x_s, y_s, z_s, \omega) \right\} dx_s dy_s. \end{aligned} \tag{4}$$

S_s is the upper (measurement) surface consisting of shots for a predicted receiver point at depth. The original/actual receiver locations on the upper surface are labeled (x', y', z') and the coordinates of the predicted receiver

at depth is now relabeled (x_g, y_g, z) in equation 4, whereas it was (x, y, z) in equation 3. $P(x_g, y_g, z, x, y, z, \omega)$ is the field corresponding to a predicted receiver at (x_g, y_g, z) and the source to (x, y, z) and change to midpoint offset $P(x_m, x_h, y_m, y_h, z_m, z_h = 0, t = 0)$ and

$$\int_{S_s} \int \int dx_s \, dy_s \, d\omega \left\{ \frac{\partial G_0^{DN}}{\partial z_s}(x, y, z, x_s, y_s, z_s, \omega) P(x_g, y_g, z, x_s, y_s, z_s, \omega) \right. \\ \left. - \frac{\partial P}{\partial z_s}(x_g, y_g, z, x_s, y_s, z_s, \omega) G_0^{DN}(x, y, z, x_s, y_s, z_s, \omega) \right\}, \quad (5)$$

and Fourier transform over x_m, x_h, y_m, y_h to find $\widetilde{P}(k_{x_m}, k_{x_h}, k_{y_m}, k_{y_h}, k_{z_m}, z_h = 0, t = 0)$. Equation 5 corresponds to the Stolt extended Claerbout imaging condition III migration for a general $v(x, y, z)$ velocity configuration, within a volume that allows two way wave propagation in terms of data only on the upper surface. In fact, equation 5 represents the generalization and extension of Claerbout III by Stolt and his colleagues, that allows migration (the original Claerbout III) to become migration-inversion.

Summary of wave equation migration for one way and two way propagating waves

Green's theorem based migration and migration-inversion require velocity information for location and all mechanical properties in the volume, V, e.g., velocity, density, and absorption for amplitude analyses at depth, respectively. When we say the medium is "known," the meaning of known depends on the goal: migration or migration-inversion. The wave prediction and imaging concepts each evolved and then extended/generalized and

merged into more complete and effective methods for imaging complex specular and non-specular structure for performing subsequent amplitude analysis. Figure 4 provides a perspective on the wave propagation and imaging evolution, respectively.

For one-way wave propagation the data from a predicted source and receiver experiment at depth, D is

$$D(\text{at depth}) = \int_{S_s} \frac{\partial G_0^{-D}}{\partial z_s} \int_{S_g} \frac{\partial G_0^{-D}}{\partial z_g} D \, dS_g \, dS_s, \tag{6}$$

where D in the integrand is the data, D(on measurement surface), $\partial G_0^{-D}/\partial z_s$ is the anticausal Green's function with Dirichlet boundary condition on the measurement surface, s connotes shot, and g, receiver, respectively. For two-way propagation, the data for a predicted source and receiver experiment at depth, D is

$$\begin{aligned} D(\text{at depth}) = \int_{S_s} \Bigg[& \frac{\partial G_0^{DN}}{\partial z_s} \int_{S_g} \left\{ \frac{\partial G_0^{DN}}{\partial z_g} D + \frac{\partial D}{\partial z_g} G_0^{DN} \right\} dS_g \\ & + G_0^{DN} \frac{\partial}{\partial z_s} \int_{S_g} \left\{ \frac{\partial G_0^{DN}}{\partial z_g} D + \frac{\partial D}{\partial z_g} G_0^{DN} \right\} dS_g \Bigg] \, dS_s, \end{aligned} \tag{7}$$

where D in the integrands is the data, D(on measurement surface). G_0^{DN} is *neither* causal nor anticausal. G_0^{DN} is not the inverse or adjoint of any physical propagating Green's function. It is the Green's function needed for WEM RTM, that is RTM based on the Stolt extended Claerbout Imaging Condition III. G_0^{DN} is the Green's function for wave propagation in the finite volume that vanishes along with its normal derivative on the lower surface and the walls. If we want to use the anticausal Green's function of

the two-way propagation with Dirichlet boundary conditions at the measurement surface then we can do that, but we will need measurements at depth (i.e., on the lower surface) and on the vertical walls to predict a source and receiver experiment at depth inside a volume with two way propagating waves. To predict the source and receiver experiment inside a volume for two-way propagation doesn't need data at depth (at a lower surface) and on the vertical sides/walls, requires a non-physical Green's function that vanishes along with its derivative on the lower surface and walls. Green's functions called upon in Green's theorem applications for migration are auxiliary functions and are specific point source wavefield solutions that satisfy the medium properties in the finite volume, and whose other properties are chosen for the convenience of the application. The commitment within Green's theorem applications is for the physical wavefield, $P(x, y, z, x_s, y_s, z_s, \omega)$, to relate to the physics of the problem and to satisfy physical boundary conditions. In contrast, the Green's function is an auxiliary function whose specific properties are chosen for the Green's theorem application and do not (in general) correspond, in any way, to a physical solution to the actual problem of interest.

In the next section, we take another step closer to our goal and objective. Having established a Stolt extended Claerbout imaging III methodology (please see equations 5 and 7) for a medium (a finite volume) with two way propagating waves, we are in a position to predict source and receiver experiments at depth and then a Stolt extended Claerbout III imaging result for data consisting of primaries and multiples.

Migrating data consisting of primaries and multiples

To determine the role and contribution of primaries and multiples in migration requires a migration method that allows two way propagation both between the source and the reflector and between the reflector and up to the receiver. For a 1D layered medium, and a normal incident wave that we will be examining, the data (consisting of primaries and internal multiples) and the results for the predicted source and receiver experiment at depth and the migration algorithm's results are all analytic, transparent and the conclusions are new, relevant and unambiguous. The role of recorded primaries and multiples in contributing first to the predicted source and receiver experiment at depth, and then to the (Stolt extended Claerbout Imaging III) coincident source and receiver experiment at time equals zero, provides a definitive response to whether or not multiples contribute to seismic imaging. Understanding the physics behind the mathematics for the case of primaries and internal multiples, allows for an immediate set of similar conclusions to be drawn for the role of free surface multiples in migration. In the section below, we provide the explicit Green's theorem source and receiver at depth prediction and then Claerbout III imaging for a general layered medium where the velocity and density vary and where the data consists of primaries and internal multiples.

Green's theorem wavefield prediction in a 1D layered medium with velocity and density variation

First, let us assume the wave propagation problem in a (one dimensional) volume V bounded by a shallower depth a and deeper depth b to be governed by the differential equation:

$$\left\{ \frac{\partial}{\partial z'} \frac{1}{\rho(z')} \frac{\partial}{\partial z'} + \frac{\omega^2}{\rho(z')c^2(z')} \right\} D(z', \omega) = 0, \tag{8}$$

where $a \leq z' \leq b$ is the depth, and $\rho(z')$ and $c(z')$ are the density and velocity fields, respectively. In exploration seismology, we let the shallower depth a be the measurement surface where the seismic acquisition takes place (please see equation 58). The volume V is the finite volume defined in the "finite volume model" for migration, the details of which can be found in Weglein et al. (2011b). We measure D at the measurement surface $z' = a$, and the objective is to predict D anywhere between the shallower surface and another surface with greater depth, $z' = b$. This can be achieved via the solution of the wave-propagation equation in the same medium by an idealized impulsive source or Green's function:

$$\left\{ \frac{\partial}{\partial z'} \frac{1}{\rho(z')} \frac{\partial}{\partial z'} + \frac{\omega^2}{\rho(z')c^2(z')} \right\} G_0(z, z', \omega) = \delta(z - z'), \tag{9}$$

where z is the location of the source, and $a < z' < b$ and z increases in a downward direction. Abbreviating $G_0(z, z', \omega)$ as G_0, the solution for D in the interval $a < z < b$ is given by Green's theorem (the generalization of

equation 58 for the case of variable velocity and density):

$$D(z,\omega) = \frac{1}{\rho(z')}\left\{D(z',\omega)\frac{\partial G_0}{\partial z'} - G_0\frac{\partial D(z',\omega)}{\partial z'}\right\}\Bigg|_{z'=a}^{z'=b}, \qquad (10)$$

where a and b are the shallower and deeper boundaries, respectively, of the volume to which the Green's theorem is applied. It is identical to equation (43) of Weglein et al. (2011b), except for the additional density contribution to the Green's theorem. Interested readers may find the derivation of equation (10) in section 2 of Liu and Weglein (2014).

Note that in equation (10), the field values on the closed surface of the volume V are necessary for predicting the field value inside V. The surface of V contains two parts: the shallower portion $z' = a$ and the deeper portion $z' = b$. In seismic exploration, the data at $z' = b$ is not available. For example, one of the significant artifacts of the current RTM procedures is caused by this phenomenon: there are events necessary for accurate wavefield prediction that reach $z' = b$ but never return to $z' = a$, as is demonstrated in Figure 5. The solution, based on Green's theorem without any approximation, was first published in Weglein et al. (2011b) and Weglein et al. (2011c). The basic idea is summarized below.

Since the wave equation that we are considering is a second-order differential equation, its general solution has a great deal of freedom/flexibility. An example of taking advantage of that freedom occurs when choosing a Green's function for many wave separation and seismic imaging procedures. For example, the most popular choice in wavefield separation is the physical solution G_0^+. In downward continuing a one way propagating upgoing

wavefield to a point in the subsurface, the anti-causal solution G_0^- is often used in equation 10 (as we have shown in the Appendices, i.e., equations 60 and 61).

Weglein et al. (2011b,c) show that (with the G_0^- choice), the contribution from (the deeper surface at) $z' = B$ will be zero under one way wave assumptions, and only measurements are required at (the shallower surface) $z' = A$. For two way propagating waves, G_0^- will not make the contribution for $z' = B$ vanish. However, if both G_0 and $\partial G_0/\partial z'$ vanish at the deeper boundary $z' = b$, where measurements are not available, then only the data at the shallower surface (i.e., the actual measurement surface) is needed in the calculation. We use G_0^{DN} to denote the Green's function with vanishing Dirichlet and Neumann boundary conditions at the deeper boundary.

Predicting the source and receiver at depth in a 1D layered medium

The original Green's theorem in equation (10) is derived to predict the wavefield (i.e., receivers) in the subsurface. It can also be used to predict the sources in the subsurface by taking advantage of reciprocity: the recording is the same after the source and receiver locations are exchanged.

Assuming we have data on the measurement surface: $D(z_g, z_s)$ (the ω dependency is ignored), we can use $G_0^{DN}(z, z_g)$ to predict it from the receiver

depth z_g to the target depth z:

$$D\left(z,z_s\right)=\frac{1}{\rho(z_g)}\left\{\frac{\partial D\left(z_g,z_s\right)}{\partial z_g}G_0^{DN}\left(z,z_g\right)-D\left(z_g,z_s\right)\frac{\partial G_0^{DN}\left(z,z_g\right)}{\partial z_g}\right\}. \tag{11}$$

Taking the $\frac{\partial}{\partial z_s}$ derivative in equation (11), we have a similar procedure to predict $\partial D(z_g,z_s)/\partial z_s$ in the subsurface:

$$\frac{\partial D\left(z,z_s\right)}{\partial z_s}=\frac{1}{\rho(z_g)}\left\{\frac{\partial^2 D\left(z_g,z_s\right)}{\partial z_g\partial z_s}G_0^{DN}\left(z,z_g\right)-\frac{\partial D\left(z_g,z_s\right)}{\partial z_s}\frac{\partial G_0^{DN}\left(z,z_g\right)}{\partial z_g}\right\}. \tag{12}$$

Equations 11 and 12 are the 1D versions of equations 3 and 4.

With equations (11) and (12), we predict the data D and its partial derivative over z_s at the subsurface location z. According to reciprocity, $D\left(z,z_s\right)=E\left(z_s,z\right)$, where $E\left(z_s,z\right)$ is resulted from exchanging the source and receiver locations in the experiment to generate D at the subsurface. The predicted data $E\left(z_s,z\right)$ can be considered as the recording of receiver at z_s for a source located at z.

For this predicted experiment, the source is located at depth z, according to Green's theorem, and we can downward continue the recording at z_s to any depth shallower than or equal to z.

In seismic migration, we predict $E\left(z_s,z\right)$ at the same subsurface depth z

Depth Range	Velocity	Density
$(-\infty, a_1)$	c_0	ρ_0
(a_1, a_2)	c_1	ρ_1
(a_2, ∞)	c_2	ρ_2

Table 1: The properties of an acoustic medium with two reflectors, at depth a_1 and a_2.

using $G_0^{DN}(z, z_s)$ to have an experiment with coincident source and receiver:

$$\begin{aligned} E(z,z) &= \frac{1}{\rho(z_s)} \left\{ \frac{\partial E(z_s,z)}{\partial z_s} G_0^{DN}(z,z_s) - E(z_s,z) \frac{\partial G_0^{DN}(z,z_s)}{\partial z_s} \right\}, \\ &= \frac{1}{\rho(z_s)} \left\{ \frac{\partial D(z,z_s)}{\partial z_s} G_0^{DN}(z,z_s) - D(z,z_s) \frac{\partial G_0^{DN}(z,z_s)}{\partial z_s} \right\}. \end{aligned} \quad (13)$$

Equation 13 is the 1D version of equation 5.

If $z_s < z_g$ and we assume the data is deghosted, the $\frac{\partial}{\partial z_s}$ operation on $D(z_g, z_s)$ is equivalent to multiplying D by $-ik$, and in this case, equation (13) can be further simplified:

$$E(z,z) = -\frac{1}{\rho(z_s)} \left\{ \frac{\partial G_0^{DN}(z,z_s)}{\partial z_s} + ikG_0^{DN}(z,z_s) \right\} D(z,z_s). \quad (14)$$

Analytic examples of migrating data with primaries and multiples (for a 1D layered medium)

As an example, for a 2-reflector model (with an ideal impulsive source located at z_s, the depth of receiver is $z_g > z_s$, the geological model is listed in Table 1), the data and its various derivatives can be expressed as:

$$
\begin{aligned}
D(z_g, z_s) &= \frac{\rho_0 x^{-1}}{2ik}\left\{y + \alpha y^{-1}\right\}, \\
\frac{\partial D(z_g, z_s)}{\partial z_g} &= \frac{\rho_0}{2} x^{-1}\left\{y - \alpha y^{-1}\right\}, \\
\frac{\partial D(z_g, z_s)}{\partial z_s} &= -\frac{\rho_0}{2} x^{-1}\left\{y + \alpha y^{-1}\right\}, \\
\frac{\partial^2 D(z_g, z_s)}{\partial z_g \partial z_s} &= \frac{\rho_0 k}{2i} x^{-1}\left\{y - \alpha y^{-1}\right\},
\end{aligned}
\tag{15}
$$

where $x = e^{ikz_s}$, $y = e^{ikz_g}$, $\sigma = e^{ikz}$, $\alpha = e^{ik(2a_1)}\left(R_1 + (1 - R_1^2)\beta\right)$, and $\beta = \sum_{n=0}^{\infty}(-1)^n R_1^n R_2^{n+1} e^{ik_1(2n+2)[a_2 - a_1]}$. And $R_1 = \frac{c_1\rho_1 - c_0\rho_0}{c_1\rho_1 + c_0\rho_0}$, and $R_2 = \frac{c_2\rho_2 - c_1\rho_1}{c_2\rho_2 + c_1\rho_1}$ are the reflection coefficients from the geological boundaries in the model.

The predicted experiment above the first reflector for Claerbout Imaging Condition III

For $z < a_1$, the boundary values of the Green's function are:

$$
\begin{aligned}
G_0^{DN}(z, z_g) &= \rho_0 \tfrac{e^{ik(z - z_g)} - e^{ik(z_g - z)}}{2ik} = \rho_0 \tfrac{\sigma y^{-1} - \sigma^{-1} y}{2ik}, \\
G_0^{DN}(z, z_s) &= \rho_0 \tfrac{\sigma x^{-1} - \sigma^{-1} x}{2ik}, \\
\tfrac{\partial G_0^{DN}(z, z_g)}{\partial z_g} &= \rho_0 \tfrac{\sigma y^{-1} + \sigma^{-1} y}{-2}, \\
\tfrac{\partial G_0^{DN}(z, z_s)}{\partial z_s} &= \rho_0 \tfrac{\sigma x^{-1} + \sigma^{-1} x}{-2}.
\end{aligned}
\tag{16}
$$

After substituting equation (15) into equation (14), we have:

$$
E(z, z) = \frac{1 + e^{ik(2a_1 - 2z)}\left(R_1 + (1 - R_1^2)\beta\right)}{2ik/\rho_0}. \tag{17}
$$

The result above can be Fourier transformed into the time domain to

obtain:

$$\frac{E(z,z,t)}{-\rho_0 c_0/2} = H(t) + R_1 H\left(t - t_1\right) + (1 - R_1^2) \times \sum_{n=0}^{\infty} (-1)^n R_1^n R_2^{n+1} H\left(t - t_1 - (2n+2)t_2\right), \tag{18}$$

where $t_1 = \frac{2a_1 - 2z}{c_0}$ and $t_2 = \frac{(a_2 - a_1)}{c_1}$. Balancing out the $-\frac{\rho_0 c_0}{2}$ factor*, the data after removing the direct wave is denoted as $\hat{D}(z,t) = \frac{-2}{\rho_0 c_0} E(z,z,t) - H(t)$:

$$\hat{D}(z,t) = R_1 H\left(t - t_1\right) + (1 - R_1^2) \sum_{n=0}^{\infty} (-1)^n R_1^n R_2^{n+1} H\left(t - t_1 - (2n+2)t_2\right). \tag{19}$$

We take the imaging condition as first letting $z \to a_1$ through values smaller than a_1, and then (subsequently) taking the limit as $t \to 0^+$, that is, approaching zero from positive values, we find:

$$\lim_{t \to 0^+} \left(\lim_{z \to a_1^-} \hat{D}(z,t) \right) = R_1, \tag{20}$$

where

$$\begin{aligned} a_1^- &= a_1 - \epsilon_1 \qquad & \epsilon_1 > 0, \\ 0^+ &= 0 + \epsilon_2 \qquad & \epsilon_2 > 0, \end{aligned} \tag{21}$$

and we obtained the image of the first reflector at the actual depth a_1 with the correct reflection coefficient as amplitude.

*This factor is present in the incident wave, i.e., the causal Green's function for a homogeneous medium with density ρ_0 and velocity c_0.

Predicting the source and receiver experiment between the first and second reflectors

For $a_1 < z < a_2$, we have:

$$\begin{aligned} G_0^{DN}(z, z_g) &= [(R_1\lambda - \lambda^{-1})\mu + (\lambda - R_1\lambda^{-1})\mu^{-1}]/[2ik_1(1+R_1)/\rho_1], \\ \frac{\partial G_0^{DN}(z, z_g)}{\partial z_g} &= [(R_1\lambda - \lambda^{-1})\mu - (\lambda - R_1\lambda^{-1})\mu^{-1}]/[2k_1(1+R_1)/(k\rho_1)], \end{aligned} \tag{22}$$

where $\lambda = e^{ik_1(z-a_1)}$, $\mu = e^{ik(z_g-a_1)}$, $k_1 = \frac{\omega}{c_1}$. Substituting equation (22) into equation (15), and transforming the aforementioned result into the time domain, we have:

$$\begin{aligned} E(z,z,t)/(-\rho_1 c_1/2) = H(t) &+ 2\sum_{n=1}^{\infty}(-1)^n R_1^n R_2^n H\{t - [2n(a_2-a_1)/c_1]\} \\ &+ \sum_{n=0}^{\infty}(-1)^{n+1} R_1^{n+1} R_2^n H\{t - [2z + 2na_2 - 2(n+1)a_1]/c_1\} \\ &+ \sum_{n=0}^{\infty}(-1)^n R_1^n R_2^{n+1} H\{t - [2(n+1)a_2 - 2na_1 - 2z]/c_1\}. \end{aligned} \tag{23}$$

Balancing out the $-\rho_1 c_1/2$ factor, the data after removing the direct wave is denoted as $\hat{D}(z,t) = \frac{-2}{\rho_1 c_1}E(z,z,t) - H(t)$:

$$\begin{aligned} \hat{D}(z,t) =& 2\sum_{n=1}^{\infty}(-1)^n R_1^n R_2^n H\{t - [2n(a_2-a_1)/c_1]\} \\ &+ \sum_{n=0}^{\infty}(-1)^{n+1} R_1^{n+1} R_2^n H\{t - [2z + 2na_2 - 2(n+1)a_1]/c_1\} \\ &+ \sum_{n=0}^{\infty}(-1)^n R_1^n R_2^{n+1} H\{t - [2(n+1)a_2 - 2na_1 - 2z]/c_1\}, \end{aligned} \tag{24}$$

and after taking the $t = 0^+$ imaging condition, we have:

$$\hat{D}(z,t) = \begin{cases} -R_1 & \texttt{if } (z = a_1 + \epsilon_1) \\ 0 & \texttt{if } (a_1 < z < a_2) \\ R_2 & \texttt{if } (z = a_2 - \epsilon_2) \end{cases}, \tag{25}$$

where $\epsilon_1, \epsilon_2 \to 0$ and then $t \to 0^+$. Note that in the previous section, i.e., to image above the first reflector at a_1, we obtain the amplitude R_1 when z approach a_1 from above. In this section we image below the first reflector at a_1, the amplitude of the image is $-R_1$ when z approaches a_1 from below, as it should.

Predicting the source and receiver experiment below the second reflector

For $z > a_1$, the boundary value of the Green's function is:

$$G_0^{DN}(z, z_g) = \frac{1}{2ik_2(1+R_1)(1+R_2)/\rho_2} \tag{26}$$
$$\times \{[\nu^{-1}(R_2\lambda - \lambda^{-1}) + R_1\nu(\lambda - R_2\lambda^{-1})]\mu + [R_1\nu^{-1}(R_2\lambda - \lambda^{-1}) + \nu(\lambda - R_2\lambda^{-1})]\mu^{-1}\},$$

where $\lambda = e^{ik_2(z-a_2)}$, $\mu = e^{ik(z_g-a_1)}$, and $\nu = e^{ik_1(a_2-a_1)}$, $k_2 = \omega/c_2$.

The result of the predicted experiment can be expressed as:

$$\begin{aligned} E(z,z) =& (\rho_2/2ik_2)[1 - R_2 e^{ik_2(2z-2a_2)} + (1-R_2^2)e^{ik_2(2z-2a_2)} \\ & \times \sum_{n=0}^{\infty} (-1)^{n+1} R_1^{n+1} R_2^n e^{ik_1(2n+2)(a_2-a_1)}]. \end{aligned} \tag{27}$$

The time domain counterpart of the equation above is:

$$E(z,z,t) = -(\rho_2 c_2/2)\{H(t) - R_2 H[t-(2z-2a_2)/c_2] + (1-R_2^2)H[t-(2z-2a_2)/c_2-(2n+2)(a_2-a_1)/c_1]. \quad (28)$$

Balancing out the $-\rho_2 c_2/2$ factor, the data after removing the direct wave is denoted as $\hat{D}(z,t) = (-2/\rho_2 c_2)E(z,z,t) - H(t)$:

$$\hat{D}(z,t) = -R_2 H[t-(2z-2a_2)/c_2] + (1-R_2^2)H[t-(2z-2a_2)/c_2-(2n+2)(a_2-a_1)/c_1], \quad (29)$$

and after taking the $t = 0^+$ imaging condition, we have:

$$\hat{D}(z,t) = \begin{cases} -R_2 & \texttt{if } (z = a_2 + \epsilon) \\ 0 & \texttt{if } (a_2 < z) \end{cases}, \quad (30)$$

where $\epsilon \to 0^+$. Note that in the previous section, i.e., to image between the first and second reflectors, we obtain the amplitude R_2 when z approach a_2 from above. In this section we image below the second reflector at a_2, the amplitude of the image is $-R_2$ when z approaches a_2 from below, as it should. Please see Figure 6.

This analysis allows us to see how the recorded events contribute to the image for source and receiver experiments above and below each reflector. At each depth, z, below the measurement surface, the predicted coincident source and receiver experiment cares about (depends on) all the actual recorded primary and multiple events on the measurement surface.

However, when the imaging condition $t = 0^+$ is applied to the coincident source and receiver experiment at depth, z, only the recorded primaries on the measurement surface contribute to the migration result at any z below the measurement surface. The conclusion: multiples do not contribute to the image at any depth.

A physical, easy to follow, and intuitive understanding of the analytic results of the previous section

In this section, we provide a geometric and physically intuitive understanding of the analytic results and conclusions of the previous section; that is, that only primaries contribute to seismic imaging.

How do the recorded events (primaries and free surface and internal multiples) contribute to: (1) the predicted source and receiver experiment at depth and (2) the image at depth that locates the reflector and then performs amplitude analysis? In this section, we examine, follow and report (for the latter two-way-wave wave migration examples) how the individual events (primaries, free surface multiples and internal multiples) each contribute to: (1) the predicted coincident source and receiver experiment at each depth, and then (2) the time equals zero imaging condition evaluation of that experiment.

The example we present provides for the first time an analysis that starts with and follows how surface recorded data (with primaries and free surface and internal multiples) influences and contributes to the subsequent coincident source and receiver experiment at depth and then imaging at each depth

level, and specifically: (1) how each individual recorded event in the surface data is involved and contributes to the new individual "events" of the predicted source and receiver experiment at each different depth, and then (2) what happens to the recorded surface event's individual contribution when applying the time equals zero imaging condition. Tracing the path that the individual surface recorded events follow (and the contribution they make) in the step by step prediction of the experiment at different depths, and then evaluating at time equals zero, is relatively easy from both the analytic derivation (provided in the previous section) and the complementary geometric and pictorial analysis that we provide in this section. The simplicity in following the role and path that individual events in the surface recorded data take in constructing the events of the source and receiver experiment at depth is due to the linearity in Green's theorem, that relates the wavefield on the surface to the wavefield inside the volume. In the three examples, a unit amplitude plane wave is normal incident on a one-D earth. The first case (please see Figures 7-9) is the example of a single reflector and a single primary, with no free surface or internal multiples. That single primary is the sole contributor to the events in the experiment above and below that single reflector. When the time equals zero condition is applied, the recorded primary is the only recorded event contributing to the experiment at depth and to the image, both below and above the reflector. Please note that (in this example) the primary and the direct wave constitute the recorded data and are used to predict the experiment at depth. The reflection data experiment at each depth comes from the total wavefield prediction at each depth minus the direct wave at that depth. That subtraction of the direct wave at

each depth to produce the reflection data at each depth corresponds to the analytic calculation in the previous section. In what follows, we always assume that the subtraction of the direct wave at each depth has taken place. For imaging above and (separately) beneath the same single (shallowest) reflector within the more general case of a layered model (provided in the previous section), where the surface reflection data consists of primaries and internal multiples, the mathematics behind the predicted experiment above and below the first reflector and the migration illustrated in Figures 7-9, is found in equations 16-30. To predict the experiment below a single reflector requires the new Stolt extended Claerbout III imaging for two way waves (described earlier in this paper, equation 7).

The second case has a single primary and a free surface multiple (please see Figures 10-12). The predicted experiment above the reflector has two surface event contributions, from the primary and the free surface multiple. When the time equals zero imaging condition is applied then only the recorded primary contributes to the image. Below the reflector the predicted experiment has two events, a primary that has a downward reflection at the reflector, and a primary from the source to the free surface and then down to the predicted receiver. The original free surface multiple in the recorded data became a primary in the predicted experiment below the reflector. Hence, the primary and free surface multiple in the recorded data became two primaries for the experiment below the reflector. However, once the time equals zero imaging condition is applied to the predicted experiment, only the recorded primary contributes to the image and the recorded multiple does not.

In the third case (please see Figures 13-17), we consider a subsurface with two reflectors and two recorded primaries and one internal multiple. As you focus on the history that each individual event in the recorded data follows and then contributes to, first in the experiment at depth and then to the image at each depth, you reach the following conclusion. Recorded primaries and free surface multiples and internal multiples all contribute to events for the predicted experiment at depth. Sometimes multiples in the recorded data even become primaries in the predicted experiment at depth. However, only the recorded primaries contribute to the image at every depth. If you removed the multiples in the recorded data, the coincident source and receiver experiment at depth would change, but once the $t = 0$ imaging condition is applied, the image's location at the correct depth or its amplitude, the reflection coefficient, will not be affected. If, in these examples, your data consisted of only multiples, you would have no image at any depth. Primaries and only primaries contribute to imaging.

The analytic example provided in explicit mathematical detail in the previous section of a 1D layered medium, with velocity and density variation, and with data consisting of primaries and internal multiples described first the prediction of a coincident source and receiver experiment at depth and then applying the time equals zero imaging condition at every depth within the layered medium. It was able to locate the reflectors and determine the exact reflection coefficient from above and from below each reflector. That calculation showed that the events in the experiment at depth depended on all the events in the surface recorded data, but once the time equals zero imaging condition is applied, to the experiment at depth, that only the

primaries in the surface recorded data contribute to the image. The recorded multiples do not contribute to the image at depth. That is the analytic counterpart that is consistent with, complements and supports the figures and descriptive geometric arguments we have just provided, in Figures 7-17. As we mentioned above, the direct wave is part of the recorded wavefield and the direct wave is a predicted event in the source and receiver experiment at depth. The direct wave in the predicted experiment is subtracted before the $t = 0$ imaging condition is applied, in both the analytic calculation in the previous section and in the pictorial description presented here.

Hence, for the purposes of imaging and inversion, primaries are signal and multiples are not.

The methods that seek to use multiples today as "signal" are really seeking to approximate images due to primaries that have not been recorded, due to limitations in acquisition, and to address the subsequent limited illumination that missing primaries can cause. They are not really using the multiple itself as an event to be followed into the subsurface for imaging purposes.

Claerbout II, RTM and the new Stolt-extended Claerbout III imaging for two way wave propagation

Let us compare Claerbout II imaging (formula 2 above) with the one-way- and two-way-wave versions of Claerbout's imaging condition III, represented in equations 6 and 7.

For Claerbout imaging condition III, for a volume with two-way-propagating

waves, given by equation 7, the sum over receivers predicts the receiver experiment at depth for a source on the measurement surface, and the sum over sources then precisely predicts the experiment with the source at the same depth. The integrations over receivers and over sources predict the source-and-receiver experiment at depth.

There is nothing ad hoc or designed to fix something amiss (as though the data or the algorithm had random noise or some deficiency, to be mitigated by stacking). The noise is algorithmic within Claerbout II and is present with exact, analytic, noise-free data in the earlier integral over receivers, as in formula 2. This is why we say Claerbout III is on the firmest physics foundation, with an interpretable, quantitative, and consistent meaning to the image. In Claerbout II "the image" comes from the constructive interference of candidate images, whereas in Claerbout III every subsurface point is directly determined to be, or not to be, structure. Once again, that clarity is why we adopt Claerbout III for analysis of the role of primaries and multiples in imaging (see Liu and Weglein, 2014 and Weglein, 2015b).

Claerbout's imaging conditions I, II, and III give equivalent imaging results for a normal-incident plane wave on a horizontal reflector. As soon as we consider prestack data for even a single horizontal reflector, however, the significant differences in image interpretability and consistency among imaging conditions become clear. Furthermore, only Claerbout III can be extended readily and naturally for amplitude analysis at specular, curved surfaces and point diffractors or pinchouts and for imaging from above and beneath a discontinuous velocity model.

The three Claerbout imaging conditions are intended and meaningful

only for primaries. However, the language and thinking behind Claerbout imaging II (and its vagueness) can be the inspiration and motivation for using the time and space coincidence of different events other than primaries, not to migrate them, but for other useful and beneficial purposes.

With a complete set of recorded primaries and a wave theory (not ray, Kirchhoff, beam, or other approximate) migration, there is in principle no illumination issue. However, when a less than complete set of primaries is recorded and/or an asymptotic migration method is used, an illumination issue will arise. We will see that under the latter circumstances, that imaging enhancement can be provided by using a recorded multiple along with a recorded primary subevent of that multiple to produce an approximate image of an unrecorded primary subevent of the multiple.

In the next section, we illustrate that process and evolution beginning with a brief and elementary review, using Claerbout II imaging to migrate a primary, followed by the method it inspired to use a Claerbout II-type method to produce an approximate image of an unrecorded primary.

Imaging primaries with Claerbout's imaging condition II

A 1D normal-incident analytic example. In this section, we use a 1D normal-incident analytic example to illustrate the idea of imaging a primary with Claerbout's imaging condition II. Let us assume that we have data from a downgoing spike wave that starts at $z = \varepsilon_s$ at $t = t_0 = 0$. The downgoing wavefield from the source side that is forward-propagated to depth z is $D =$

$\exp(i\omega[(z-\varepsilon_s)/c_0])$, whereas the upgoing wavefield from the receiver side that is back-propagated to depth z is $U = R_1 \exp(i\omega[(d-\varepsilon_s)/c_0+(d-z)/c_0])$, where R_1 and d are the reflection coefficient and the depth of the reflector, respectively (Figure 18). Applying Claerbout's imaging condition II, we have

$$\begin{aligned} I_P &= \int \exp\left(-i\omega\left[\frac{z-\varepsilon_s}{c_0}\right]\right) \times R_1 \exp\left(i\omega\left[\frac{d-\varepsilon_s}{c_0}+\frac{d-z}{c_0}\right]\right) d\omega \\ &= \int R_1 \exp\left(-i\omega\left[\frac{2d-2z}{c_0}\right]\right) d\omega \\ &= \pi c_0 R_1 \delta(z-d). \end{aligned} \tag{31}$$

We obtain the correct image location at depth d with an amplitude of $\pi c_0 R_1$.

Using a multiple to approximately image an unrecorded primary

1D normal-incident analytic example. Now we apply Claerbout's imaging condition II to a seismic data set that contains a first-order free-surface multiple. Again, we assume a downgoing spike wave that is at $z = \varepsilon_s$ at $t = t_0 = 0$ (Figure 19). A first-order free-surface multiple is recorded at z_g. The downgoing wavefield from a "virtual source" (represented by the dashed red line in Figure 19) that is forward-propagated to depth z is $D = -R_1 \exp(i\omega[(d-\varepsilon_s)/c_0 + (d+z)/c_0])$. The upgoing wavefield from the receiver side (represented by the yellow dashed line in Figure 19) that is back-propagated to depth z is $U = -R_1^2 \exp(i\omega[(d-\varepsilon_s)/c_0 + 2d/c_0 + (d-z)/c_0])$.

Here, we have assumed the downward reflection coefficient at the free-surface to be -1 in deriving the up and down wavefields (Figure 19). Applying the time and space coincidence of these two wavefields, we have

$$I_M = \int \left(-R_1 \exp\left(-i\omega\left[\frac{d-\varepsilon_s}{c_0} + \frac{d+z}{c_0}\right]\right)\right) \times \left(-R_1^2 \exp\left(i\omega\left[\frac{d-\varepsilon_s}{c_0} + \frac{2d}{c_0} + \frac{d-z}{c_0}\right]\right)\right) d\omega$$
$$= \int R_1^3 \exp\left(-i\omega\left[\frac{2d-2z}{c_0}\right]\right) d\omega = \pi c_0 R_1^3 \delta(z-d). \qquad (32)$$

We obtain the correct image location at depth d, but with a different amplitude of $\pi c_0 R_1^3$ rather than $\pi c_0 R_1$. This procedure can provide an approximate image of a primary subevent if the velocity of the primary subevent can be estimated. This simple example can be extended readily to the case of the two different primary subevents, in which the velocity of the unrecorded primary subevent will allow for its approximate image.

In Figure 20 (a), we see an example where the subevent primaries of the multiple experience velocities c_0 and c_1, and c_0, respectively. Let d_1 be the depth of the shallower reflector and d_2 the depth of the deeper reflector, respectively. The travel time, t_1, of the (downgoing at z_1) subevent in Figure 20 (b) is

$$t_1 = \frac{d_1 - \epsilon_s}{c_0} + \frac{2(d_2 - d_1)}{c_1} + \frac{d_1 + z_1}{c_0}$$

and the travel time of the (upgoing at z_1) multiple in Figure 20 (a) is

$$t_2 = t_1 + \left(\frac{d_1 - z_1}{c_0} + \frac{d_1 - z_1}{c_0}\right).$$

To predict the receiver on the upfield at the z_1 to a deeper depth z_2 requires multiplying the field at z_1 by $\exp(-i(\omega/c_0)(z_2 - z_1))$. Likewise, to predict the downfield at z_2, where $z_2 > z_1$, from the downfield at z_1 requires multiplying the upfield at z_1 by $\exp(i(\omega/c_0)(z_2 - z_1))$. Those two operations are illustrated in Figure 20 (c). The amplitude of the approximate image of the unrecorded primary is $(R_2')^2 R_1$ rather than R_1, where $R_2' = R_2 T_{01} T_{10}$.

Hence, the space and time coincidence of the up and downwave procedure (in the use of multiples) only depends on and uses the velocity of the primary that has not been recorded, c_0. The subevent of the multiple [in Figure 20 (d) (ABCD)] and its history, and the velocities it has experienced play absolutely no role in the procedure. If the multiple had a subevent illustrated in Figure 20 (e) rather than the subevent in Figure 20 (b), then, once again, the operation is $\exp(i(\omega/c_0)(z_2 - z_1))$ on ABCDEFGH and $\exp(-i(\omega/c_0)(z_2 - z_1))$ on ABCDEFGHIJ. How can such a process of using the multiple ever be considered "migrating the multiple". To consider this process "migrating the multiple" would mean that migration doesn't care about the history of the event being migrated. This process cares about the velocity of the unrecorded primary, and produces an approximate image of that event. All conventional migration concepts Claerbout I, II and III require the detailed velocity history of the event being migrated. The multiple is being useful but it is not being migrated.

The methods that seek to use multiples today as "signal" are in fact seeking to approximate images resulting from primaries that were not recorded because of limitations in acquisition and then are seeking to address the subsequent, limited illumination that missing primaries can cause. The methods

are not using the multiple itself as an event to be followed into the subsurface for imaging purposes. Figure 21 illustrates the idea.

Assume that a multiple is recorded and a primary that is a subevent is also recorded. The idea is to extract and predict, from the recorded multiple and the recorded primary, the image representing an unrecorded subevent primary. All the various incarnations that use multiples as "signal" actually and entirely are attempting to obtain the approximate image of an unrecorded primary. It is the missing image of unrecorded primaries that the methods seek to produce and to use. Such a use of multiples is a testament to the fact that a complete set of primaries is sufficient for imaging the subsurface. Using a multiple to achieve an approximate image of an unrecorded primary can provide an enhanced image because of a more complete set of images of primaries and is not migration of the multiples.

Weglein (2014a) presents field data examples from PGS in which clear, compelling added value was demonstrated for the image from primaries, combined with the approximate images of unrecorded primaries, in comparison with the image from the original primaries. Also see Whitmore et al. (2010), Valenciano et al. (2014), and Chao Ma and Yanglei Zou (2015) for examples of using multiples to enhance imaging. The figure (21) illustrates the idea.

Assume a multiple is recorded, and a long offset primary that is a subevent is also recorded. The idea is to extract and predict the image due to an unrecorded primary, e.g., at a smaller offset, from the recorded multiple and the recorded longer offset primary. All the various incarnations that are using multiples as "signal" are actually, and entirely after removing a

recorded longer offset primary to have the output as a shorter offset unrecorded primary. It's the missing image of unrecorded primaries that the method is seeking to produce and to utilize.

The recipe of taking the multiples back in time and the primaries forward in time and arranging for Imaging Condition II (not III) produces that output. However, that procedure is not migrating the multiples, in any sense or interpretation of the meaning of migration and as we have demonstrated definitely not migrating the multiple as an event.

In a Recent Advances and the Road Ahead presentation, "Multiples: signal or noise?", Weglein (2014b) (please see `https://vts.inxpo.com/scripts/Server.nxp?LASCmd=L:0&AI=1&ShowKey=21637&LoginType=0&InitialDisplay=1&ClientBrowser=0&DisplayItem=NULL&LangLocaleID=0&RandomValue=1415030021699`) showed a field data example, from PGS, where there was clear added-value demonstrated beyond actual primaries for shallow structural improvement, plus the approximate images of unrecorded primaries predicted from using multiples, compared to the image from the original primaries.

There is another issue: in order to predict a free surface or internal multiple, the primary sub-events that constitute the multiple must be in the data, for the multiple prediction method to recognize an event as a multiple. (Please see, e.g., Weglein et al., 2003.) If the short offset primary is not recorded, the multiple that is composed of the short and long offset multiple will not be predicted as a multiple. That issue and basic contradiction within the method is recognized by those who practice this method, and instead of predicting the multiple, they use all the events in the recorded data, primaries and multiples. The multiples that are within the data can

be useful for predicting approximate images of missing primaries but the primaries in the data will cause artifacts. There are other artifacts that also come along with this method that have been noted in the literature (see, e.g., Weglein, 2015b).

The reality of today's methods for using multiples to predict missing "primaries" are aimed at structural improvement, at best, and are not claiming, seeking or delivering the amplitude and phase fidelity of the predicted primary. Those who go so far as to advocate using fewer sources and/or more widely separated cables because recorded multiples can produce "something like" a missing primary need to understand the deficits and costs including generating so-called cross-talk artifacts, less effectiveness with deeper missing primaries and the amplitude fidelity of the predicted primary. Whether the tradeoff makes sense ought to depend on, in part, the depth of the target, the type of play, and whether a structural interpretation or amplitude analysis is planned within a drilling program and decision.

By the way, this entire wave equation migration analysis (Claerbout Imaging Condition III) is ultimately based on the idea from Green (1828) that to predict a wave (an experiment) inside a volume you need to know the properties of the medium in the volume.

There is an alternative view: The inverse scattering series method communicates that all processing objectives can be achieved directly and without subsurface information. The inverse scattering series treat multiples as a form of coherent noise, and provide distinct subseries to remove free surface and internal multiples before the inverse scattering subseries for imaging and inversion achieve their goals using only primaries (Weglein et al., 2003 and

Weglein et al., 2012). If the inverse scattering series (the only direct multi-dimensional inversion method) needed multiples to perform migration and inversion, it would not have provided subseries that remove those multiply reflected events.

With a velocity model (the most definitive, capable, physically interpretable and general imaging principle, the extended Claerbout III by Stolt and colleagues) or without a velocity model (inverse scattering series imaging) only primaries are signal, in the sense that they are the only events called upon to locate and delineate targets. If you want to consider a multiple as a conditional 'signal', that can at times enhance imaging, there is no harm in that. But to say that multiples are being migrated, and/or are the same footing as primaries, is simply not true and relates more to marketing, than to a realistic view of the role that primaries and multiples play in seismic exploration. A complete set of recorded primaries, processed with a wave theory migration (versus asymptotic or ray migration) would not need or benefit from multiples. Multiples need to be removed before performing a velocity analysis and a velocity model is required by all the methods that seek to use multiples to enhance imaging. Another question: what if the assumed unrecorded primary event in the method is actually recorded. Will the image of the recorded primary and the image of the approximate version of the recorded primary from the multiple damage the image of the actual primary, that has been assumed to not have been recorded?

Conclusions

There is considerable interest in the topic of "multiples: signal or noise" with e.g., the July 2015 TLE issue having a special section devoted to that subject. That special TLE section contained contributions with a diverse set of viewpoints on that subject. This paper provides an examination, analysis and set of conclusions on the role that primaries and multiples play in determining subsurface information from recorded seismic reflection data.

Migration and migration-inversion are the methods used to extract subsurface information from seismic data. In this paper, we describe various imaging conditions, and then we extend the most physically well-founded, definitive, and complete imaging principle, the prediction of a coincident source and receiver experiment at depth at time equals zero, to a volume that has two way wave propagation, both for: (1) the wave propagating from the source and to the reflector, and (2) for the wave propagating from the reflector to the receiver and (3) that assumes up and downgoing waves at every point in a smoothly varying velocity model. Providing among other benefits (beyond the immediate and parochial interests of this paper), a fundamentally more capable, interpretable and effective migration method, in comparison with the current leading edge industry RTM.

A first migration method that is equally effective at all frequencies at the reservoir

If this new two way wave migration method (equation 7) is implemented with a Green's function for the velocity and density configuration inside the volume with Dirichlet and Neumann boundary conditions at the lower surface of the volume, that will avoid asymptotic high frequency assumptions in both the imaging principle and the way it is implemented. For a smooth velocity model it will allow for two way propagation at every point (with part of the wave moving up and part moving down at every point) in addition to allowing for overall two way propagation between, both source and reflector, and also between the reflector and receiver. That will allow for a migration result that is equally effective at all frequencies at the reservoir. That in turn will allow the recent advances in broad band data collection and processing to deliver its benefit at the target.

The current RTM is based on the ad hoc and less well-founded imaging principle; the space and time coincidence of up-waves from the reflector and down-waves from the source. The imaging condition behind all current RTM migration methods has a travel time curve ingredient with ray based candidate images and, hence, the imaging condition itself makes an intrinsic high frequency assumption or approximation. The predicted experiment at depth imaging condition is not a high frequency assumption or approximation. In addition, it is the only imaging condition that can be extended to accommodate the location and inversion of both specular (predicting the angle dependent plane wave reflection coefficient, and not a geometric optics

approximate) and for non-specular reflectors where that migration method extends the imaging model to a point reflectivity/point scatterer model, for imaging and inverting, for example, curved, diffractive and pinch-out targets. Imaging with that new two way wave propagation migration method is effective both above and below a reflector, without causing (or needing to address) so-called backscatter or "rabbit ears" when migrating with RTM Claerbout II with a discontinuous velocity model. The predicted source and receiver experiment at depth imaging condition is not a high frequency asymptotic concept or construct.

With that well-founded imaging principle combined with the new method to predict the experiment at depth inside a volume with two way propagating waves, we provide an analytic example of imaging and inverting a data set consisting of primaries and multiples, inside a layered one dimensional medium. The predicted experiment at every depth has its own events that are linear combinations of all the events in the recorded data. However, when the time equals zero imaging condition is called upon, then the migrated result only depends on the primaries in the recorded data. The multiples play absolutely no role in the imaging or migration. That analysis assumed the velocity model was discontinuous and known. For a continuous velocity model the multiples will produce false images (for both Claerbout II and Claerbout III migration) that can masquerade as and/or interfere with the actual structure determined from migrating primaries. Since, in practice, we employ smooth velocities when we migrate, multiples must be removed before imaging for processing goals that seek to effectively locate and invert reflections. For the most physically well-founded, capable, and

interpretable seismic imaging and inversion principles and methods the conclusion is that multiples were, are, and will remain unambiguously noise that need to be effectively removed before the migration and migration-inversion of primaries.

However, we show that there are circumstances when the recording of primaries is inadequate or incomplete, and multiples can be used to isolate and approximately migrate an unrecorded sub-event primary of the multiple. That ad hoc Claerbout II inspired procedure will produce a lower level and less capable form of migration for the unrecorded primary than migrating an actual recorded primary would provide with Claerbout II migration. It provides a lower level of information, and in practice is often confined to help with extending shallow structure but without amplitude interpretability, or the ability to produce a plane wave reflection coefficient for a specular reflection, or to image and invert non-specular reflections. In addition, the use of multiples produces a new form of algorithmic produced coherent noise called cross-talk. For the most effective and capable migration and inversion algorithms of recorded primaries, multiples are coherent noise that must be removed. Multiples need to be removed to migrate recorded primaries. To find an approximate image of an unrecorded primary requires being able to predict multiples.

For a lower bar, level and tier of information bearing, and signal, we can consider multiples as a conditional form and source of decipherable information that contributes to a more complete set of primaries and signal, since they can provide an approximate image of an unrecorded primary. Multiples can be a source of approximate signal, when real signal is missing,

but as an entity and event, they are never signal. Primaries are signal and when multiples can provide an approximate image of an unrecorded primary, they can be useful. Multiples themselves are never migrated.

We discuss below how much attention and investment we recommend for removing or using multiples. Both are very important, and need to be encouraged. However, the removal of multiples that are interfering with primaries, for an unknown and complex multidimensional subsurface, remains a key open issue, and high priority pressing challenge, and frequent impediment and obstruction to effective on-shore and off-shore exploration and production drilling decisions.

While the use of multiples to provide the approximate image of an unrecorded primary can be important and useful for extending shallow structure, we cannot allow that to distract from the priority and much higher impact that would be delivered by addressing the pressing need for a next level of multiple removal capability (see e.g. Weglein et al., 2011a and Weglein, 2015b). Recorded primaries have the greatest potential for providing subsurface information. Multiples need to be removed to image recorded primaries.

Primaries are the only events that are migrated for structural and amplitude analysis. In practice, to migrate primaries, with any migration method, requires multiples to first be removed.

The role of multiples in the inverse scattering series

The inverse scattering series allows all processing objectives to be achieved directly and without subsurface information. The inverse scattering series is the only direct inversion method for a multidimensional subsurface. There are distinct task specific subseries of the inverse scattering series that remove free surface and internal multiples. There are other subseries that input primaries to determine structure and perform amplitude analysis (e.g., Weglein et al., 2003, and Weglein et al., 2012). If multiples were needed for migration and inversion the inverse scattering series would not allow subseries that remove them. The inverse scattering series, a direct inversion machine, treats multiples as coherent noise that needs to be removed. The distinct free surface multiple elimination subseries (Carvalho et al., 1992; Weglein et al., 1997) and internal multiple attenuation subseries (Araújo et al., 1994; Weglein et al., 1997) and internal multiple elimination subseries for a 1D subsurface (Yanglei Zou and Weglein, 2015) represent the currently most capable methods for removing multiples. However, issues remain, and interfering primaries and multiples in a multi-dimensional subsurface remains an open issue and challenge. A proposed strategy to provide an effective response to that prioritized and pressing challenge was proposed (see, e.g., Weglein et al., 2011a; Weglein, 2015a) but much serious work and effort remains before a comprehensive solution is available. That issue often arises in offshore plays and frequently occurs in both conventional and unconventional on-shore plays.

The inability to effectively remove a multiple interfering with a reservoir

primary precludes (or impedes) many important exploration and production plays, and opportunities, often contributing to dry hole drilling and suboptimal development well placement. The current most capable strategy consisting of an ISS internal multiple attenuator plus adaptive subtraction can and will damage a target reservoir primary that interferes with a multiple. Damaging a target primary is an extremely serious issue, and processors and interpreters will often leave in the interfering multiple proximal to or intersecting a reservoir primary rather than risk damaging or destroying a target primary.

The use of multiples to provide an approximate image of an unrecorded primary, while useful, cannot be used to distract from the prioritized and pressing need to provide more effective multiple removal capability and thereby allowing recorded primaries to deliver their full promise and value.

We recommend focusing the most attention on the most important problem, and not to be distracted or discouraged by the difficulty of solving the most significant problem, or taken off track by a more convenient, trendy, and less impactful pursuit. Providing the next level of multiple removal capability is a tough and daunting problem, but it is the essential prioritized high impact problem today, that needs to be, and will be addressed. That advance in multiple removal effectiveness will allow many currently inaccessible, precluded or too high risk offshore plays and on-shore conventional and unconventional plays and opportunities to become accessible, and currently accessible targets to become better delineated and defined.

Acknowledgements

M-OSRP sponsors are thanked for their encouragement and support. The author would like to thank John Etgen, Jeff Shragge, Nizar Chemingui, Dan Whitmore and Alejandro Valenciano (PGS), Robert H. Stolt (ConocoPhillips, retired), Clement Kostov and Richard Coates (Schlumberger), Scott Morton (Hess) and Fred Hoffman (Bluescape) for constructive and worthwhile discussions that benefited this paper. The author gratefully acknowledges PGS for examples showing how multiples can be used to predict approximate images of unrecorded primaries, and Lundin Malaysia and PETRONAS for show-rights in an invited 2014 SEG RARA presentation by the author. I would like to thank Yi Luo and Tim Keho (Saudi Aramco) and David Monk and Bill Goodway (Apache Corp.) for stimulating and useful discussions that motivated and benefited this paper. The author thanks Jinlong Yang, Fang Liu, Chao Ma, Jing Wu, Yanglei Zou, Qiang Fu, and Xinglu Lin for assistance in preparing this paper. I would like to express my gratitude and appreciation to Jim Mayhan for his invaluable assist and support in preparing and editing this paper.

References

Amundsen, L., 1994, The propagator matrix related to the Kirchhoff-Helmholtz integral in inverse wavefield extrapolation: Geophysics, **59**, 1902–1910.

Araújo, F. V., A. B. Weglein, P. M. Carvalho, and R. H. Stolt, 1994, Inverse scattering series for multiple attenuation: An example with surface and

internal multiples: 64th Annual International Meeting, SEG, Expanded Abstracts, 1039–1041.

Carvalho, P. M., A. B. Weglein, and R. H. Stolt, 1992, Nonlinear inverse scattering for multiple suppression: Application to real data. Part I: 62nd Annual International Meeting, SEG, Expanded Abstracts, 1093–1095.

Claerbout, J. F., 1971, Toward a unified theory of reflector mapping: Geophysics, **36**, 467–481.

Clayton, R. W., and R. H. Stolt, 1981, A Born-WKBJ inversion method for acoustic reflection data: Geophysics, **46**, 1559–1567.

Green, G., 1828, An essay on the application of mathematical analysis to the theories of electricity and magnetism: Privately published. (Available at `http://babel.hathitrust.org/cgi/pt?id=hvd.yl131n;view=1up;seq=9`).

Liu, F., and A. B. Weglein, 2014, The first wave equation migration RTM with data consisting of primaries and internal multiples: theory and 1D examples: Journal of Seismic Exploration, **23**, 357–366.

Ma, C., and Y. Zou, 2015, A clear example using multiples to enhance and improve imaging: Comparison of two imaging conditions relevant to this analysis: The Leading Edge, **34**, 814–816.

Morse, P. M., and H. Feshbach, 1981, Methods of theoretical physics: Feshbach Publishing, LLC. (Original publication 1953 by The McGraw-Hill Companies, Inc.).

Schneider, W. A., 1978, Integral formulation for migration in two and three dimensions: Geophysics, **43**, 49–76.

Stolt, R. H., 1978, Migration by Fourier transform: Geophysics, **43**, 23–48.

Stolt, R. H., and A. K. Benson, 1986, Seismic migration: theory and practice: Geophysical Press.

Stolt, R. H., and A. B. Weglein, 1985, Migration and inversion of seismic data: Geophysics, **50**, 2458–2472.

———, 2012, Seismic imaging and inversion: Application of linear inverse theory: Cambridge University Press.

Valenciano, A. A., S. Crawley, E. Klochikhina, N. Chemingui, S. Lu, and D. Whitemore, 2014, Imaging complex structures with separated Up- and Down-going wavefields: 84th Annual International Meeting, SEG, Expanded Abstracts, 3941–3945.

Weglein, A. B., 2014a, Multiples: Signal or noise? Invited presentation given at the SEG Convention special session on Recent advances and the road ahead, Denver, Colorado.

———, 2014b, Multiples: signal or noise?: 84th Annual International Meeting, SEG, Expanded Abstracts, 4393–4399.

———, 2015a, Multiple removal: open issues, pressing challenges and recent progress towards providing the next and higher level of required capability: 85th Annual International Meeting, SEG, Expanded Abstracts, 4555–4562.

———, 2015b, Primaries — the only events that can be migrated and for which migration has meaning: The Leading Edge, **34**, 808–813.

Weglein, A. B., F. V. Araújo, P. M. Carvalho, R. H. Stolt, K. H. Matson, R. T. Coates, D. Corrigan, D. J. Foster, S. A. Shaw, and H. Zhang, 2003, Inverse scattering series and seismic exploration: Inverse Problems, **19**, R27–R83.

Weglein, A. B., F. A. Gasparotto, P. M. Carvalho, and R. H. Stolt, 1997, An inverse-scattering series method for attenuating multiples in seismic reflection data: Geophysics, **62**, 1975–1989.

Weglein, A. B., S.-Y. Hsu, P. Terenghi, X. Li, and R. H. Stolt, 2011a, Multiple attenuation: Recent advances and the road ahead (2011): The Leading Edge, **30**, 864–875.

Weglein, A. B., F. Liu, X. Li, P. Terenghi, E. Kragh, J. D. Mayhan, Z. Wang, J. Mispel, L. Amundsen, H. Liang, L. Tang, and S.-Y. Hsu, 2012, Inverse scattering series direct depth imaging without the velocity model: first field data examples: Journal of Seismic Exploration, **21**, 1–28.

Weglein, A. B., and R. H. Stolt, 1999, Migration-inversion revisited (1999): The Leading Edge, **18**, 950–952, 975.

Weglein, A. B., R. H. Stolt, and J. D. Mayhan, 2011b, Reverse-time migration and Green's theorem: Part I — The evolution of concepts, and setting the stage for the new RTM method: Journal of Seismic Exploration, **20**, 73–90.

———, 2011c, Reverse time migration and Green's theorem: Part II — A new and consistent theory that progresses and corrects current RTM concepts and methods: Journal of Seismic Exploration, **20**, 135–159.

Whitmore, N. D., A. A. Valenciano, W. Sollner, and S. Lu, 2010, Imaging of primaries and multiples using a dual-sensor towed streamer: 80th Annual International Meeting, SEG, Expanded Abstracts, 3187–3192.

Zhang, Y., S. Xu, N. Bleistein, and G. Zhang, 2007, True-amplitude, angle-domain, common-image gathers from one-way wave-equation migrations: Geophysics, **72**, S49–S58.

Zou, Y., and A. B. Weglein, 2015, An internal-multiple elimination algorithm for all first-order internal multiples for a 1D earth: 85th Annual International Meeting, SEG, Expanded Abstracts, 4408–4412.

Appendix I: The infinite hemispherical migration model

The earliest wave equation migration pioneers considered the subsurface volume (where the source and receiver experiment would be predicted) as an infinite hemispherical half space with known mechanical properties, whose upper plane surface corresponded to the measurement surface, as in, *e.g.*, Schneider (1978) and Stolt (1978). See Figure 1.

Those two papers each made a tremendous conceptual and practical contribution to seismic imaging and exploration seismology. However, there are several problems with the infinite hemispherical migration model. That model assumes: (1) that all subsurface properties beneath the measurement surface (MS) are known, and (2) that an anticausal Green's function (*e.g.*, Schneider (1978)), with a Dirichlet boundary condition on the measurement surface, would allow measurements (MS) of the wavefield, P, on the upper plane surface of the hemisphere to determine the value of P within the hemispherical volume, V. The first assumption leads to the contradiction that we have not allowed (for the purposes and objectives of seismic exploration and processing) for anything that is unknown to be determined in our model, since everything within the closed and infinite hemisphere is assumed to

be known. Within the infinite hemispherical model there is nothing and/or nowhere below the measurement surface where an unknown scattering point or reflection surface can serve to produce reflection data whose generating reflectors are initially unknown and being sought by the migration process.

The second assumption, in early infinite hemispherical wave equation migration, assumes that Green's theorem with wavefield measurements on the upper plane surface and using an anticausal Green's function satisfying a Dirichlet boundary condition can determine the wavefield within V. That conclusion assumes that the contribution from the lower hemispherical surface of S vanishes as the radius of the hemisphere goes to infinity. That is not the case, as we explicitly demonstrate below. To examine the various large radius hemispherical surface contributions to Green's theorem wave prediction in a volume, it is instructive to review the relationship between Green's theorem and the Lippmann-Schwinger scattering equation.

Appendix II: Green's theorem review

We begin with a space and time domain Green's theorem. Consider two wavefields P and G_0 that satisfy

$$(\nabla^2 - \frac{1}{c^2}\partial_t^2)P(\mathbf{r},t) \quad = \quad \rho(\mathbf{r},t) \tag{33}$$

and

$$(\nabla^2 - \frac{1}{c^2}\partial_t^2)G_0(\mathbf{r},t,\mathbf{r}',t') \quad = \quad \delta(\mathbf{r}-\mathbf{r}')\delta(t-t'), \tag{34}$$

where we assume 3D wave propagation and the wavefield velocity c is a constant. ρ is a general source, *i.e.*, it represents both active sources (air guns, dynamite, vibrator trucks) and passive sources (heterogeneities in the earth). The causal solution to equation 33 can be written as

$$P(\mathbf{r},t) = \int_{-\infty}^{t^+} dt' \int_{\infty} d\mathbf{r}' \rho(\mathbf{r}',t') G_0^+(\mathbf{r},t,\mathbf{r}',t'), \tag{35}$$

where G_0^+ is the causal whole space solution to equation 34 and $t^+ = t + \epsilon$ where ϵ is a small positive quantity. The integral from t^+ to ∞ is zero due to the causality of G_0^+ (please see Morse and Feshbach, 1981, page 836). Equation 35 represents the linear superposition of causal solutions G_0^+ with weights $\rho(\mathbf{r}',t')$ summing to produce the physical causal wavefield solution to equation 33. Equation 35 is called the scattering equation and represents an all space and all time causal solution for $P(\mathbf{r},t)$. It explicitly includes all sources and produces the field at all points of space and time. No boundary or initial conditions are required in equation 35.

Now consider the integral

$$\begin{aligned} &\int_0^{t^+} dt' \int_V d\mathbf{r}' (P\nabla'^2 G_0 - G_0 \nabla'^2 P) \\ &= \int_0^{t^+} dt' \int_V d\mathbf{r}' \nabla' \cdot (P\nabla' G_0 - G_0 \nabla' P), \end{aligned} \tag{36}$$

and we rewrite equation 36 using Green's theorem

$$\begin{aligned}&\int_0^{t^+} dt' \int_V d\mathbf{r}' \nabla' \cdot (P\nabla' G_0 - G_0 \nabla' P)\\ =&\int_0^{t^+} dt' \oint_S dS' \hat{n} \cdot (P\nabla' G_0 - G_0 \nabla' P).\end{aligned} \tag{37}$$

This is essentially an identity, within the assumptions on functions and surfaces, needed to derive Green's theorem. Now choose $P = P(\mathbf{r}', t')$ and $G_0 = G_0(\mathbf{r}, t, \mathbf{r}', t')$ from equations 33 and 34. Then replace $\nabla'^2 P$ and $\nabla'^2 G_0$ from the differential equations 33 and 34.

$$\nabla'^2 G_0 = \frac{1}{c^2}\partial_t'^2 G_0 + \delta(\mathbf{r} - \mathbf{r}')\delta(t - t') \tag{38}$$

$$\nabla'^2 P = \frac{1}{c^2}\partial_t'^2 P + \rho(\mathbf{r}', t'), \tag{39}$$

and assume that the output variables $(\mathbf{r}, t)$ are in the intervals of integration: $\mathbf{r}$ in V, $t > 0$. The left hand side of equation 36 becomes:

$$\begin{aligned}&\int_0^{t^+} dt' \int_V d\mathbf{r}' \frac{1}{c^2}(P\partial_{t'}^2 G_0 - G_0 \partial_{t'}^2 P) + P(\mathbf{r}, t)\\ -&\int_0^{t^+} dt' \int_V d\mathbf{r}' \rho(\mathbf{r}', t') G_0(\mathbf{r}, t, \mathbf{r}', t').\end{aligned} \tag{40}$$

The expression inside the first set of parentheses is a perfect derivative

$\partial_{t'}(P\partial_{t'}G_0 - G_0\partial_{t'}P)$ integrated over t'. The result is (for $\mathbf{r}$ in V and $t > 0$)

$$\begin{aligned} P(\mathbf{r},t) = &\int_V d\mathbf{r}' \int_0^{t^+} dt' \rho(\mathbf{r}',t') G_0(\mathbf{r},t,\mathbf{r}',t') \\ &- \frac{1}{c^2}\Big|_{t'=0}^{t^+} \int_V d\mathbf{r}' [P\partial_{t'}G_0 - G_0\partial_{t'}P] \\ &+ \int_0^{t^+} dt' \oint_S dS' \hat{n} \cdot (P\nabla' G_0 - G_0 \nabla' P). \end{aligned} \tag{41}$$

We assumed differential equations 38 and 39 in deriving equation 41 and G_0 can be any solution of equation 38 in the space and time integrals in equation 36, causal, anticausal, or neither. Each term on the right hand side of equation 41 will differ with different choices of G_0, but the sum of the three terms will always be the same, $P(\mathbf{r},t)$.

If we now choose G_0 to be causal ($= G_0^+$) in equation 41, then in the second term on the right hand side the upper limit gives zero because G_0^+ and $\partial_{t'}G_0^+$ are zero at $t' = t^+$. The causality of G_0^+ and $\partial_{t'}G_0^+$ causes only the lower limit $t' = 0$ to contribute in

$$-\frac{1}{c^2}\Big|_{t'=0}^{t^+} \int_V d\mathbf{r}' [P\partial_{t'}G_0^+ - G_0^+\partial_{t'}P]. \tag{42}$$

If we let the space and time limits in equation 41 both become unbounded, *i.e.*, $V \to \infty$ and the t' interval becomes $[-\infty, t^+]$, and choose $G_0 = G_0^+$, the whole space causal Green's function, then by comparing equations 35 and 41 we see that for $\mathbf{r}$ in V and $t > 0$ that

$$\int_{-\infty}^{t^+} dt' \oint_S dS' \hat{n} \cdot (P \nabla' G_0^+ - G_0^+ \nabla' P)$$
$$- \frac{1}{c^2} \Big|_{-\infty}^{t^+} \int_{\infty} d\mathbf{r}' [P \partial_{t'} G_0^+ - G_0^+ \partial_{t'} P] = 0, \tag{43}$$

where $V = \infty$ means a volume that spans all space.

The solution for $P(\mathbf{r}, t)$ in equation 35 expresses the fact that if all of the factors that both create the wavefield (active sources) and that subsequently influence the wavefield (passive sources, *e.g.*, heterogeneities in the medium) are explicitly included in the solution as in equation 35, then the causal solution is provided explicitly and linearly in terms of those sources, as a weighted sum of causal solutions, and no surface, boundary or initial conditions are necessary or required.

Boundary conditions and initial conditions allow for influences outside the volume and time interval of interest, respectively, to influence the solution for the field inside the volume of space and interval of time of interest.

In the $(\mathbf{r}, \omega)$ domain equations 33 and 34 become

$$(\nabla^2 + k^2) P(\mathbf{r}, \omega) = \rho(\mathbf{r}, \omega) \tag{44}$$
$$(\nabla^2 + k^2) G_0(\mathbf{r}, \mathbf{r}', \omega) = \delta(\mathbf{r} - \mathbf{r}'), \tag{45}$$

where $\int_{-\infty}^{\infty} P(\mathbf{r}, t) e^{i\omega t} dt = P(\mathbf{r}, \omega)$ and $\int_{-\infty}^{\infty} G_0(\mathbf{r}, \mathbf{r}', t) e^{i\omega t} dt = G_0(\mathbf{r}, \mathbf{r}', \omega)$, and t' is chosen to be zero in equation 38. The causal all space and temporal

frequency solution analogous to equation 35 is

$$P(\mathbf{r},\omega) = \int_{\infty} d\mathbf{r}' \rho(\mathbf{r}',\omega) G_0^+(\mathbf{r},\mathbf{r}',\omega), \tag{46}$$

and Green's second identity is

$$\int_V d\mathbf{r}' (P\nabla'^2 G_0 - G_0 \nabla'^2 P) = \oint_S dS'\, \hat{n} \cdot (P\nabla' G_0 - G_0 \nabla' P). \tag{47}$$

Substituting $\nabla^2 G_0 = -k^2 G_0 + \delta$ and $\nabla^2 P = -k^2 P + \rho$ in Green's theorem , we find

$$\left.\begin{array}{l} P(\mathbf{r},\omega) \\ \mathbf{r}\ in\ V \\ \\ 0 \\ \mathbf{r}\ out\ V \end{array}\right\} = \int_V d\mathbf{r}' P(\mathbf{r}',\omega)\delta(\mathbf{r}-\mathbf{r}')$$
$$= \int_V \rho(\mathbf{r}',\omega) G_0(\mathbf{r},\mathbf{r}',\omega)\, d\mathbf{r}' + \oint_S (P\nabla' G_0 - G_0 \nabla' P)\cdot \hat{n}\, dS. \tag{48}$$

There are no initial conditions (temporal boundary conditions), since in $\mathbf{r},\omega$ we have already explicitly included all time in Fourier transforming from t to ω. In $\mathbf{r},\omega$ the only issue in equation 48 is whether sources are inside or outside V. The Lippmann-Schwinger equation (46) provides the causal physical solution for P for all $\mathbf{r}$ due to the sources in all space. Equation 46 is the $\mathbf{r},\omega$ version of equation 35 and must choose $G_0 = G_0^+$ (causal) to have P as the physical solution built from the superposition (and linearity of weighted elementary causal solution, $G_0^+(\mathbf{r},\mathbf{r}',\omega)$). In contrast, equation 48

(as in equation 41) will produce the physical solution, P, with any solution for G_0 that satisfies equation 45.

Equation 46 can be written as:

$$\int_V \rho\, G_0^+ + \int_{\infty - V} \rho\, G_0^+. \tag{49}$$

where $\infty - V$ corresponds to the volume outside V. Assume that among the infinite number of solutions for G_0 that satisfy equation 45, we choose in equation 48, the causal solution G_0^+. Then for $\mathbf{r}$ in V, the second term on the right hand side of equation 48 (with choosing $G_0 = G_0^+$ in equation 48) equals the second term in equation 49, *i.e.*,

$$\int_{\infty - V} d\mathbf{r}' \rho G_0^+ = \oint_S dS' \hat{n} \cdot (P \nabla' G_0^+ - G_0^+ \nabla' P). \tag{50}$$

Thus, the first term in equation 49 gives contribution to P, for $\mathbf{r}$ in V due to sources in V, and the second term in equation 49 gives contribution to P, for $\mathbf{r}$ in V due to sources not in V. With $G_0 = G_0^+$

$$\oint_S dS' \hat{n} \cdot (P \nabla' G_0^+ - G_0^+ \nabla' P), \tag{51}$$

provides the contribution to the field, P, inside V due to sources outside the volume V.

What about the large $|\mathbf{r}|$ contribution of the surface integral to the field inside the volume? We use Green's theorem to predict that the contribution to the physical/causal solution P in V from the surface integral in Green's

theorem, in general, and also

$$\oint_S \{P\frac{\partial G_0^+}{\partial n} - G_0^+\frac{\partial P}{\partial n}\}dS, \tag{52}$$

vanishes as $|\mathbf{r}| \to \infty$ and in contrast the contribution to P in V from

$$\oint_S \{P\frac{\partial G_0^-}{\partial n} - G_0^-\frac{\partial P}{\partial n}\}dS, \tag{53}$$

does not vanish as $|\mathbf{r}| \to \infty$.

We begin with equation 48

$$\left.\begin{array}{c} P(\mathbf{r},\omega) \\ \mathbf{r}\ in\ V \\ \\ 0 \\ \mathbf{r}\ out\ V \end{array}\right\} = \int_V d\mathbf{r}'\rho(\mathbf{r}',\omega)G_0^{\pm}(\mathbf{r},\mathbf{r}',\omega) + \oint_S dS'\{P\frac{\partial G_0^{\pm}}{\partial n} - G_0^{\pm}\frac{\partial P}{\partial n}\} \tag{54}$$

with G_0 either causal G_0^+ or anticausal G_0^-. Taking the limit $|\mathbf{r}| \to \infty$, then for $G_0 = G_0^+$ in 54, the contribution from the second term on the right hand side of equation 54 to P in V must go to zero, following a comparison with

$$P(\mathbf{r},\omega) = \int_\infty d\mathbf{r}'\rho(\mathbf{r}',\omega)G_0^+(\mathbf{r},\mathbf{r}',\omega), \tag{55}$$

(the Lippmann-Schwinger equation). However, with $G_0 = G_0^-$, and as $|\mathbf{r}| \to \infty$,

$$\begin{aligned} &\oint_{S\to\infty} dS'\{P\frac{\partial G_0^-}{\partial n} - G_0^-\frac{\partial P}{\partial n}\} + \int_{V\to\infty} d\mathbf{r}'\rho(\mathbf{r}',\omega)G_0^-(\mathbf{r},\mathbf{r}',\omega) \\ &= \int_{V\to\infty} d\mathbf{r}'\rho(\mathbf{r}',\omega)G_0^+(\mathbf{r},\mathbf{r}',\omega) + 0, \end{aligned} \tag{56}$$

so

$$\oint_{S\to\infty}\{P\frac{\partial G_0^-}{\partial n}-G_0^-\frac{\partial P}{\partial n}\}dS$$
$$=\int_\infty[G_0^+(\mathbf{r},\mathbf{r}',\omega)-G_0^-(\mathbf{r},\mathbf{r}',\omega)]\rho(\mathbf{r}',\omega)d\mathbf{r}'\neq 0 \qquad (57)$$

for all $\mathbf{r}$. Hence, the large distance surface contribution to the physical field, P, within V with the surface values of the physical field P and $\partial P/\partial n$ and an anticausal Green's function G_0^- will not vanish as $|\mathbf{r}|\to\infty$. As we mentioned earlier, this non-vanishing of the surface integral equation 53 at large distances with an anticausal G_0 is one of the problems with the infinite hemispherical model of seismic migration.

That non-vanishing contribution from the hemisphere as $|\mathbf{r}|\to\infty$, combined with the fact that the infinite hemisphere model assumes the entire subsurface, down to "infinite" depth is known, suggests the need for a different model. That model is the finite volume model (see, *e.g.*, Weglein et al., 2011b;c).

Appendix III: Finite volume model for migration

The finite model for migration assumes that we know or can adequately estimate earth medium properties (*e.g.*, velocity) down to the reflector we seek to image. The finite volume model assumes that beneath the sought after reflector the medium properties are, and can remain, unknown. The "finite volume model" corresponds to the volume within which we assume the earth properties are known and within which we predict the wavefield from surface

measurements. The finite volume model addresses the two problematic issues of the infinite hemisphere model, *i.e.*, (1) the assumption that we know the subsurface to all depths and (2) the (**erroneous**) assumption that the contribution from the lower hemispherical surface, of the closed surface (as $|\mathbf{r}| \to \infty$) to the surface integral, with an anticausal Green's function, has no contribution to the field being predicted in the volume.

The finite volume model removes both of the problematic assumptions behind the infinite hemisphere model. However, we are now dealing with a finite volume V, and with a surface S, consisting of upper surface S_U, lower surface S_L and walls, S_W (Figure 2). We only have measurements on S_U. In the following sections on: (1) Green's theorem for one-way propagation; and (2) Green's theorem for two-way propagation, we show how the choice of distinct and appropriate Green's function allows the finite volume migration model to be realized for a volume with one-way or two way propagating waves. The construction of the Green's function that can accommodate two-way propagation in V, from contributions only on S_U, is a new contribution (Weglein et al., 2011b;c) that allows Claerbout Imaging III to be realized in a volume with two-way propagating waves. That places RTM on a firm wave theoretical Green's theorem basis, for the first time, with algorithmic consequence and with a clear mathematical physics understanding of the amplitude of the RTM image. The new Green's function is neither causal, anticausal, nor a combination of causal and/or anticausal Green's functions. In the important paper by Amundsen (1994), a finite volume model for wavefield prediction is developed which requires knowing (*i.e.*, predicting through solving an integral equation) for the wavefield at

the lower surface. In the next sections, we show that for one and two-way propagation, respectively, that with a proper and distinct choice of Green's function, in each case, that absolutely no wavefield measurement information on the lower surface is required or needs to be estimated/predicted. Below, we review how to choose the Green's functions that allow for two-way propagation (for RTM application) without the need for measurements on the lower boundary of the closed surface in Green's theorem.

Appendix IV: Finite volume model for migration: Green's theorem for predicting the source and receiver experiment for one way waves

Consider a 1D upgoing plane wavefield $P = Re^{-ikz}$ propagating upward through the 1D homogeneous volume without sources between $z = a$ and $z = b$ (Figure 3). The wave P inside V can be predicted from boundary values of P and dP/dz using

$$P(z,\omega) \;=\; \Big|_{z'=a}^{b} \{P(z',\omega)\; \frac{dG_0}{dz'}(z,z',\omega) - G_0(z,z',\omega)\frac{dP}{dz'}(z',\omega)\} \qquad (58)$$

with a Green's function, G_0, that satisfies

$$\left(\frac{d^2}{dz'^2} + k^2\right)\; G_0(z,z',\omega) \;=\; \delta(z-z') \qquad (59)$$

for z and z' in V. To be more precise in our language, we want to predict what a receiver at depth would record in terms of what a surface receiver

records. We can easily show that for an upgoing wave, $P = Re^{-ikz}$, that if in equation 58 one chooses $G_0 = G_0^+$ (causal, $e^{ik|z-z'|}/(2ik)$), the lower surface (i.e. $z' = b$) predicts P in V and the contribution from the upper surface vanishes. On the other hand, if we choose $G_0 = G_0^-$ (anticausal solution $e^{-ik|z-z'|}/(-2ik)$), then the upper surface $z = a$ provides $P = Re^{-ikz}$ in V and there is no contribution from the lower surface $z' = b$. The effective sources $(P(b), P'(b))$ on the lower surface $z' = b$ with a causal Green's function, G_0^+, will produce a wave moving away from the source at $z = b$, hence upward in the region between $a < z < b$. At the upper surface $z' = a$, the anticausal G_0^- will produce waves moving towards the source at $z = a$ and hence moving upward for $a < z < b$. Also, using the anticausal Green's function, G_0^-, in equation 58 takes the wavefield, P (and its derivative, P') at $z = a$, and predict where it was previously at earlier time. For an upwave in $a < z < b$, the prediction of where (and what) the wave at $z = a$ was previously is predicting the wave between $z = a$ and $z = b$.

Since in exploration seismology the reflection data is typically upgoing, once it is generated at the reflector, and we only have measurements at the upper surface $z' = a$, we choose an anticausal Green's function G_0^- in one-way wave prediction in the finite volume model. If, in addition, we want to remove the need for dP/dz' at $z' = a$ we can impose a Dirichlet boundary condition on G_0^-, to vanish at $z' = a$. The latter Green's function is labeled

G_0^{-D},

$$G_0^{-D} \;=\; -\frac{e^{-ik|z-z'|}}{2ik} - \left(-\frac{e^{-ik|z_I-z'|}}{2ik}\right), \tag{60}$$

where z_I is the image of z through $z' = a$. It is easy to see that $z_I = 2a - z$ and that

$$P(z) \;=\; -\frac{dG_0^{-D}}{dz'}(z, z', \omega)\Big|_{z'=a} P(a) \;=\; e^{-ik(z-a)}P(a), \tag{61}$$

in agreement with a simple Stolt FK phase shift for predicting an upward propagating wave in a volume, that is between $a < z < b$ in terms of the wavefield at $z = a$. Please note that $P(z, \omega) \;=\; -dG_0^{-D}/dz'(z, z', \omega)|_{z'=a} P(a, \omega)$ back propagates $P(z' = a, \omega)$, not G_0^{-D}. The latter thinking that G_0^{-D} back propagates (or G_0^{+D} forward propagates) data is a fundamental mistake/flaw in many seismic back propagation migration and inversion theories (and in feedback multiple attenuation methods), that harkens back to the historically earlier and qualitative Huygens principle concepts that preceded Green's theorem to amplitude issues and errors.

Green's theorem 3D generalization that predicts an experiment with both sources and receivers at depth for a one way propagating wavefield

in the volume is as follows:

$$\begin{aligned}
& \int \frac{dG_0^{-D}}{dz_s}(x'_s, y'_s, z'_s, x_s, y_s, z_s; \omega) \\
& \times \left[\int \frac{dG_0^{-D}}{dz_g}(x'_g, y'_g, z'_g, x_g, y_g, z_g; \omega) D(x'_g, y'_g, z'_g, x'_s, y'_s, z'_s; \omega) dx'_g dy'_g \right] dx'_s dy'_s \\
= \; & M(x_s, y_s, z_s, x_g, y_g, z_g; \omega) \\
= \; & M(x_m, y_m, z_m, x_h, y_h, z_h; \omega), \qquad (62)
\end{aligned}$$

where $x_g + x_s = x_m$, $y_g + y_s = y_m$, $z_g + z_s = z_m$, $x_g - x_s = x_h$, $y_g - y_s = y_h$, and $z_g - z_s = z_h$. In the space and time domain, equation 62 corresponds to "uncollapsed migration", $M(x_m, y_m, z_m, x_h, y_h, z_h = 0; t = 0)$ that extends and generalizes the original Imaging Condition III, to non-zero offset at time equals zero. The retaining of k_h information (rather than stacking over k_h, for $x_h = 0$, hence, uncollapsed) allows for imaging and subsequent AVO analysis in a multi-D subsurface. The extension and generalization of Claerbout Imaging III to allow structure and amplitude analysis was pioneered by Stolt and his colleagues (see *e.g.* Clayton and Stolt (1981), Stolt and Weglein (1985), Weglein and Stolt (1999), Stolt and Weglein (2012)).

For one way propagating wavefields in the finite volume, choosing an anticausal Green's function allows only wavefield measurements on the upper surface to be sufficient to predict the wavefield in the volume. For two way propagating wavefields in a finite volume an anticausal Green's function will not allow for measurements on the upper surface to be sufficient to predict the wavefield in the volume. The Green's function for two-way propagation

that will eliminate the need for data at the lower surface of the closed Green's theorem surface is found by finding a general solution to the Green's function for the medium in the finite volume model and imposing both Dirichlet and Neumann boundary conditions at the lower surface.

For predicting a two way propagating wavefield inside a volume, the references that provide the background and explicit analytic examples of how to arrange a Green's function and its normal derivative to vanish at the lower surface of the surface integral [e.g., equations 47, 58] we refer the reader to Weglein et al. (2011b), Weglein et al. (2011c), and F. Liu and Weglein (2014).

Figures

Figure 1: *The infinite hemispherical migration model. The measurement surface is denoted by MS.*

Figure 2: *A finite volume model.*

Figure 3: *1D upgoing plane wavefield.*

Figure 4: *Backpropagation model evolution.*

Figure 5: *Green's theorem predicts the wavefield at an arbitrary depth z between the shallower depth a and deeper depth b.*

Figure 6: *Imaging with primaries and internal multiples. A double Green's theorem is utilized with the data, and a Green's function that along with its normal derivative vanishes on the lower surface (and on the walls, in multi-D). That is what wave-equation migration means for waves that are two-way propagating in the medium.*

Figure 7: *Case 1: a primary from a single reflector (recorded data).*

Figure 8: *Case 1: a primary from a single reflector. Above the reflector (predicted experiment at depth).*

Figure 9: *Case 1: a primary from a single reflector. Below the reflector (predicted experiment at depth).*

Figure 10: *Case 2: a primary and a free-surface multiple (recorded data).*

Figure 11: *Case 2: a primary and a free-surface multiple. Above the reflector (predicted experiment at depth).*

Figure 12: *Case 2: a primary and a free-surface multiple. Below the reflector (predicted experiment at depth).*

Figure 13: *Case 3: two primaries and an internal multiple (recorded data).*

Figure 14: *Case 3: two primaries and an internal multiple. Above the first reflector (predicted experiment at depth).*

Figure 15: *Case 3: two primaries and an internal multiple. Below the first reflector (predicted experiment at depth).*

Figure 16: *Case 3: two primaries and an internal multiple. Above the second reflector (predicted experiment at depth).*

Figure 17: *Case 3: two primaries and an internal multiple. Below the second reflector (predicted experiment at depth).*

Figure 18: *Use of a primary to find an image. Down-going wave that starts at* $z = \varepsilon_s$ *at* $t = t_0 = 0$.

Figure 19: *Use of a multiple to find an approximate image of an unrecorded primary.*

Figure 20:

Figure 21: *The multiple is used to find a missing primary. Primaries are what migration and inversion call for and utilize. For the mathematical details, please see Weglein (2015b).*

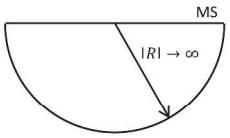

The infinite hemispherical migration model. The measurement surface is denoted by MS.
279x361mm (300 x 300 DPI)

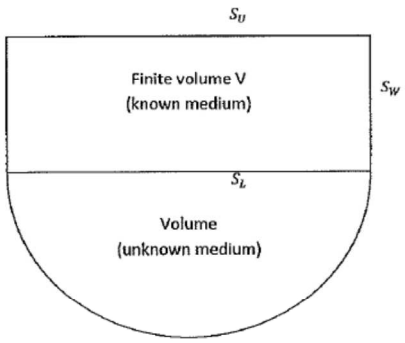

A finite volume model.
279x361mm (300 x 300 DPI)

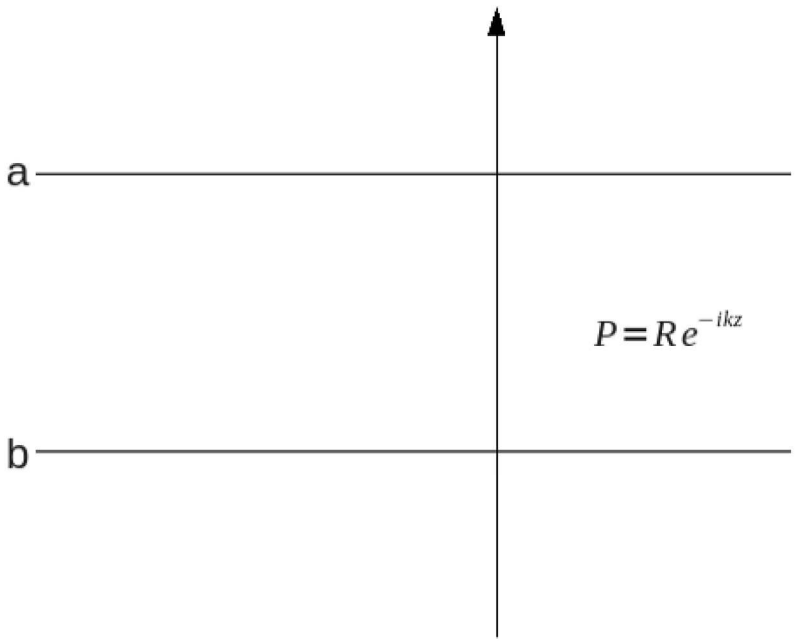

1D upgoing plane wavefield.
209x148mm (300 x 300 DPI)

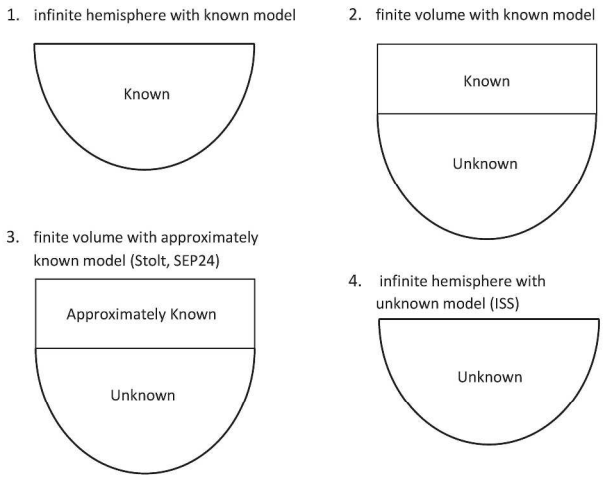

Backpropagation model evolution.
279x361mm (300 x 300 DPI)

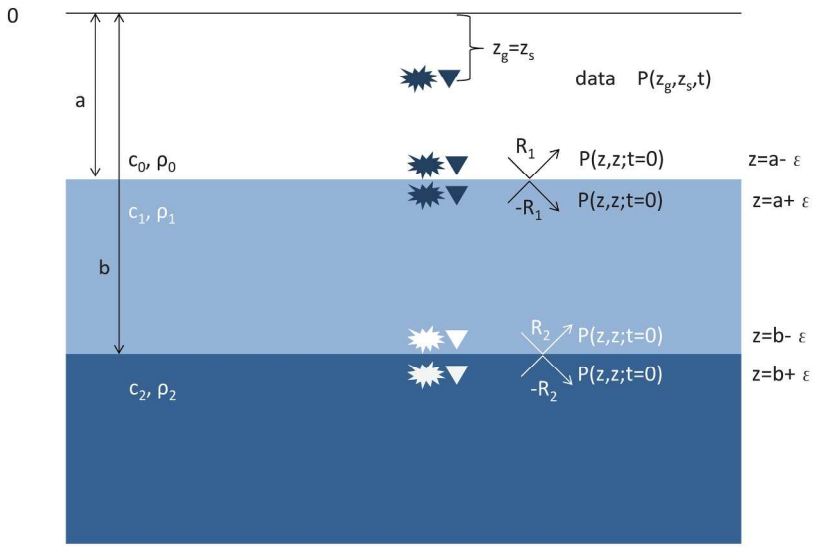

Green's theorem predicts the wavefield at an arbitrary depth z between the shallower depth a and deeper depth b.
215x166mm (300 x 300 DPI)

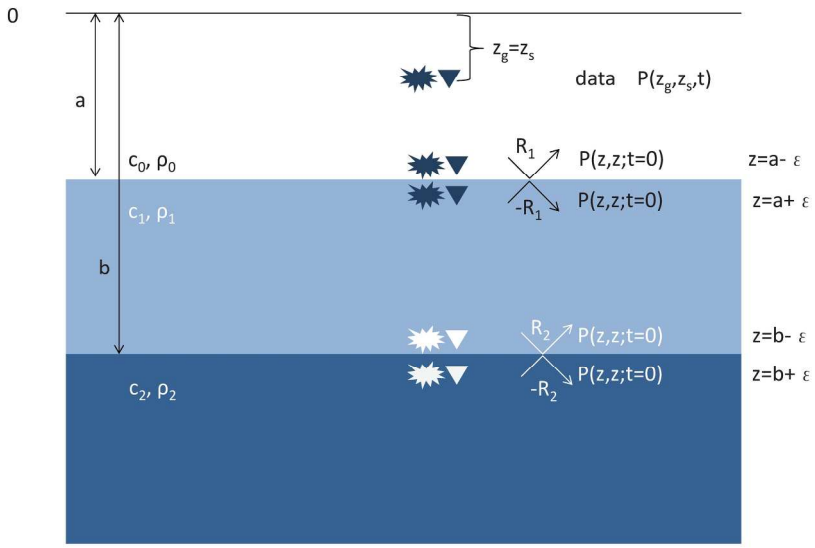

Imaging with primaries and internal multiples. A double Green's theorem is utilized with the data, and a Green's function that along with its normal derivative vanishes on the lower surface (and on the walls, in multi-D). That is what wave-equation migration means for waves that are two-way propagating in the medium.
215x166mm (300 x 300 DPI)

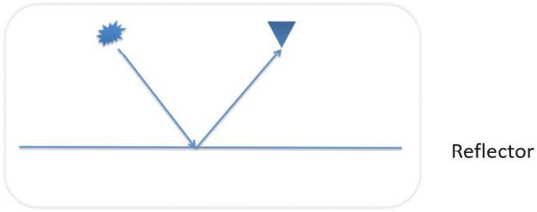

Case 1: a primary from a single reflector (recorded data).
215x166mm (300 x 300 DPI)

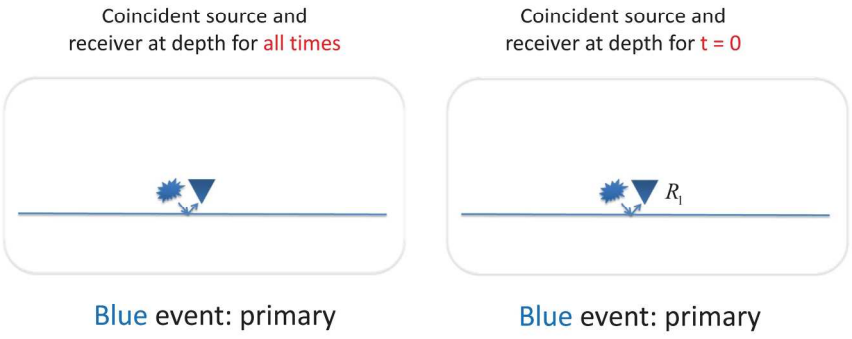

Case 1: a primary from a single reflector. Above the reflector (predicted experiment at depth).
215x166mm (300 x 300 DPI)

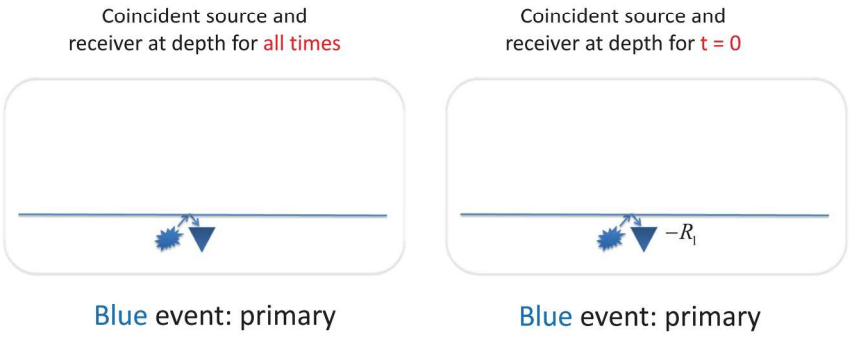

Case 1: a primary from a single reflector. Below the reflector (predicted experiment at depth).
215x166mm (300 x 300 DPI)

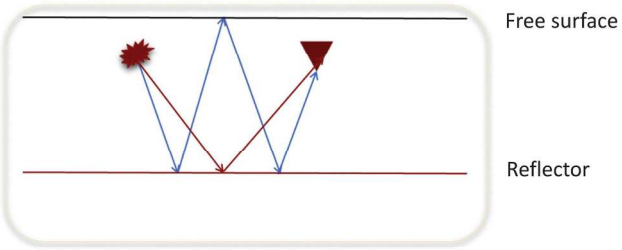

Red event: primary
Blue event: free-surface multiple

Case 2: a primary and a free-surface multiple (recorded data).
215x166mm (300 x 300 DPI)

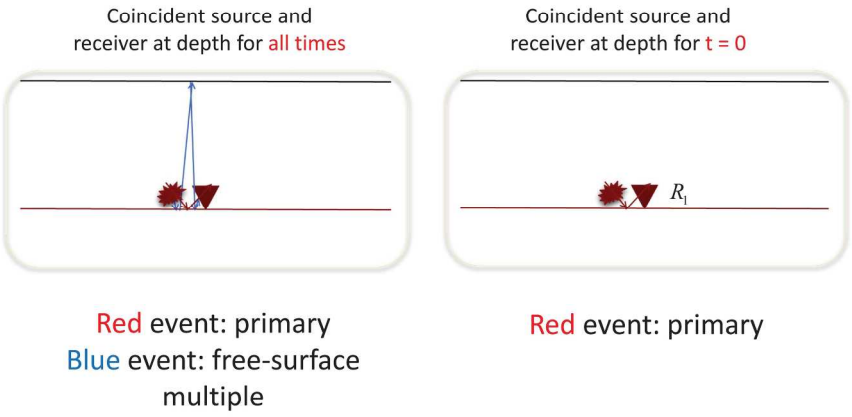

Case 2: a primary and a free-surface multiple. Above the reflector (predicted experiment at depth).
215x166mm (300 x 300 DPI)

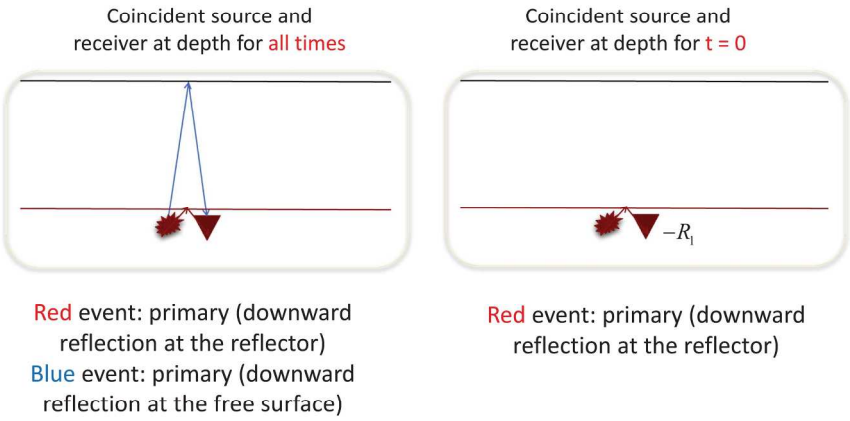

Case 2: a primary and a free-surface multiple. Below the reflector (predicted experiment at depth).
215x166mm (300 x 300 DPI)

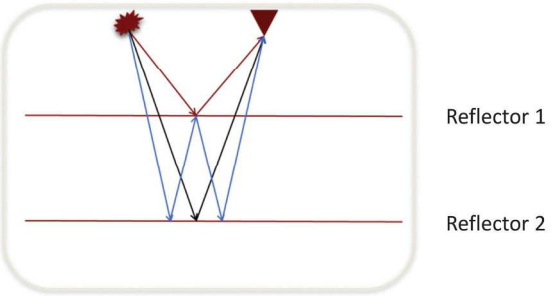

Red event: primary from the first reflector
Black event: primary from the second reflector
Blue event: internal multiple

Case 3: two primaries and an internal multiple (recorded data).
215x166mm (300 x 300 DPI)

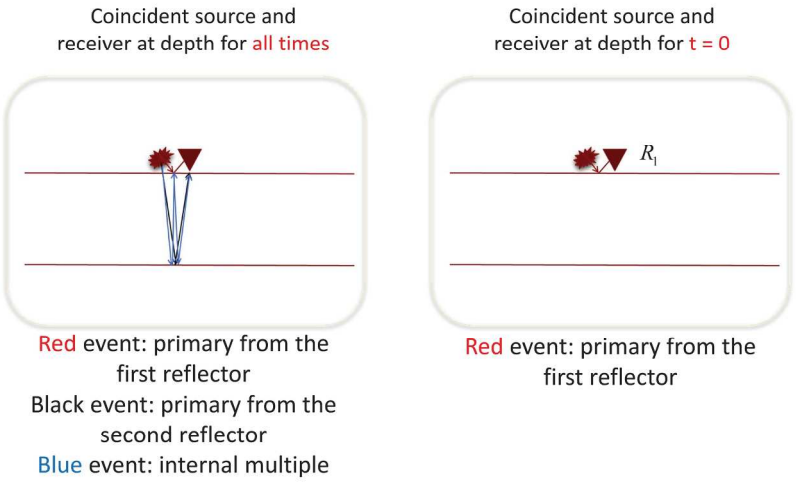

Case 3: two primaries and an internal multiple. Above the first reflector (predicted experiment at depth).
215x166mm (300 x 300 DPI)

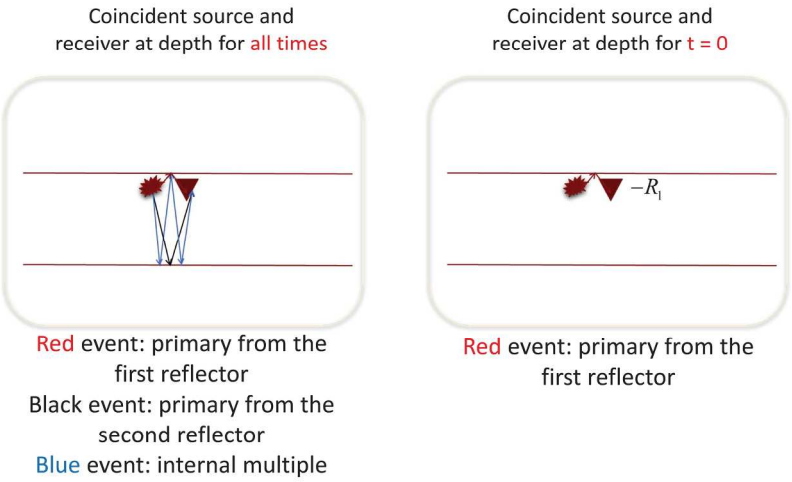

Case 3: two primaries and an internal multiple. Below the first reflector (predicted experiment at depth).
215x166mm (300 x 300 DPI)

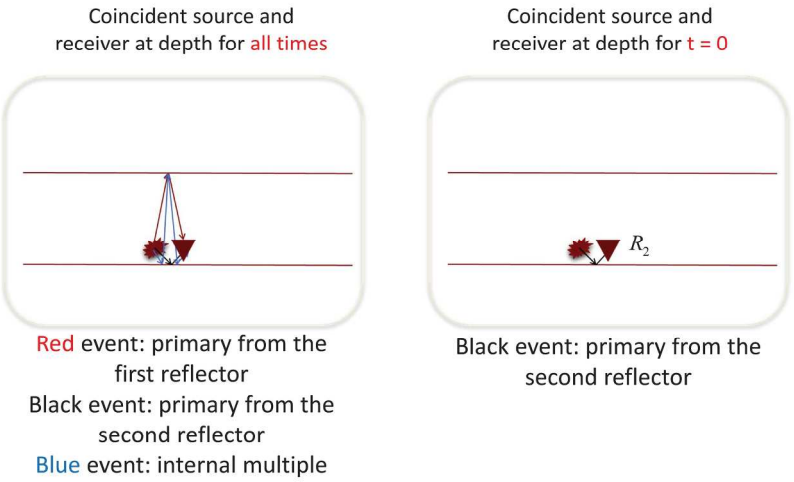

Case 3: two primaries and an internal multiple. Above the second reflector (predicted experiment at depth).
215x166mm (300 x 300 DPI)

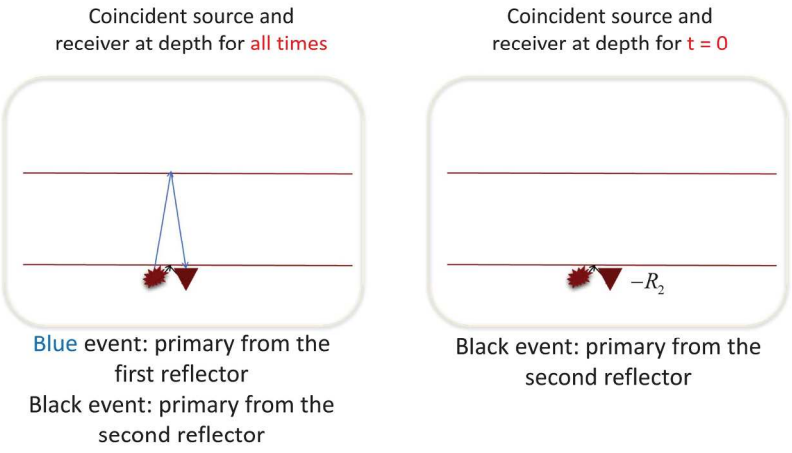

Case 3: two primaries and an internal multiple. Below the second reflector (predicted experiment at depth).
215x166mm (300 x 300 DPI)

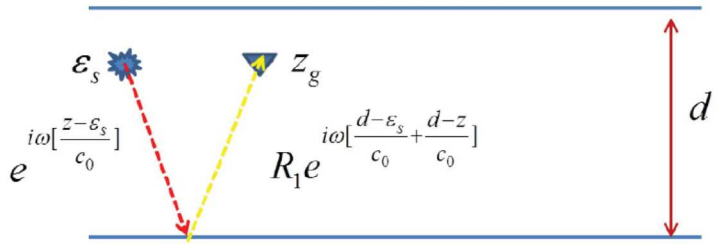

Use of a primary to find an image. Down-going wave that starts at $z=\varepsilon_s$ $t=t\_0=0$.
279x361mm (300 x 300 DPI)

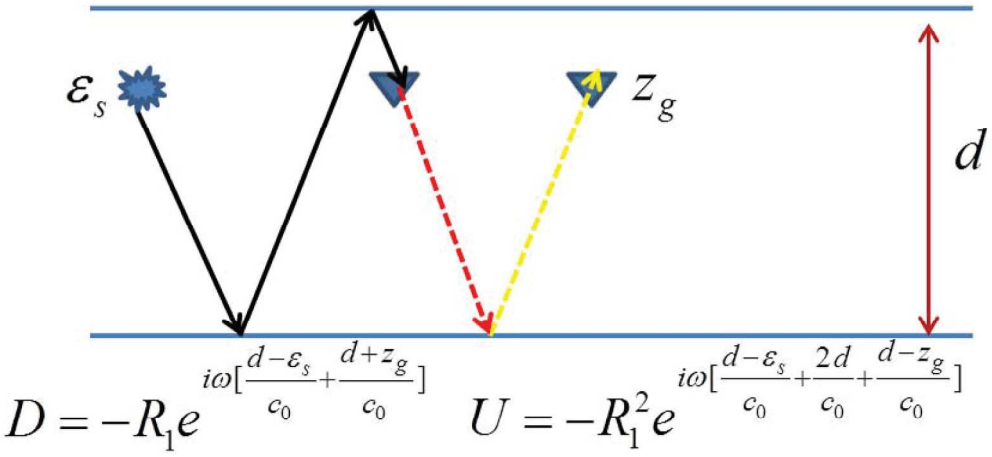

Use of a multiple to find an approximate image of an unrecorded primary.
215x166mm (300 x 300 DPI)

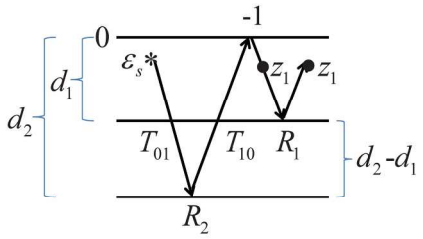

215x166mm (300 x 300 DPI)

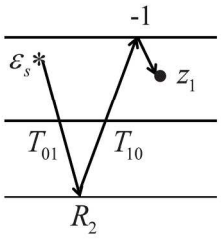

215x166mm (300 x 300 DPI)

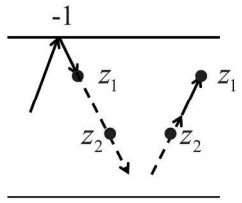

215x166mm (300 x 300 DPI)

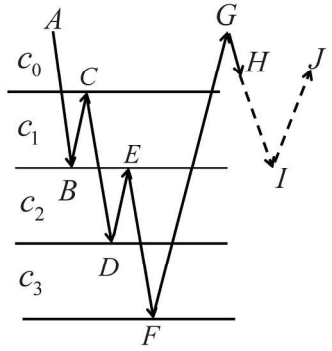

215x166mm (300 x 300 DPI)

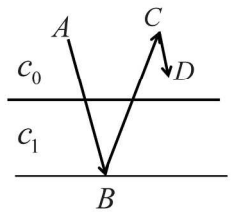

215x166mm (300 x 300 DPI)

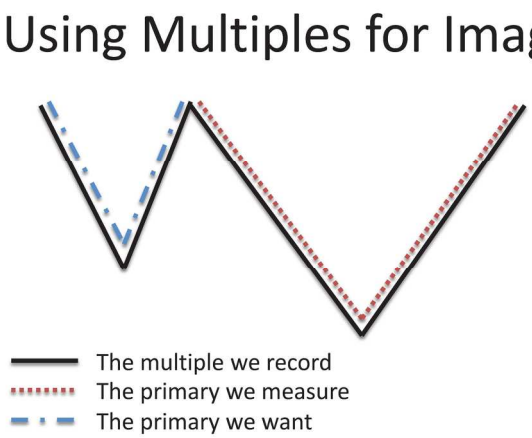

The multiple is used to find a missing primary. Primaries are what migration and inversion call for and utilize. For the mathematical details, please see Weglein (2015b).
190x142mm (300 x 300 DPI)